

1 **This article is a preprint published at EarthArXiv**

2 **Notice - From the AMS Copyright Policy section 7c:**

3 This work is under review at the Journal of Climate. Copyright in this work may be
4 transferred without further notice. This work has not yet been peer-reviewed and is pro-
5 vided by the contributing author(s) as a means to ensure timely dissemination of schol-
6 arly and technical work on a noncommercial basis. Copyright and all rights therein are
7 maintained by the author(s) or by other copyright owners. It is understood that all per-
8 sons copying this information will adhere to the terms and constraints invoked by each au-
9 thor's copyright. This work may not be reposted without explicit permission of the copy-
10 right owner. [https://www.ametsoc.org/index.cfm/ams/publications/ethicalguidelines- and-ams-](https://www.ametsoc.org/index.cfm/ams/publications/ethicalguidelines-and-ams-policies/ams-copyright-policy)
11 [policies/ams-copyright-policy.](https://www.ametsoc.org/index.cfm/ams/publications/ethicalguidelines-and-ams-policies/ams-copyright-policy)

12 **Terrestrial evaporation and global climate: lessons from Northland, a planet**
13 **with a hemispheric continent**

14 Marysa M. Laguë*

15 *Department of Earth and Planetary Science, University of California Berkeley, Berkeley, CA,*
16 *USA, and University of Saskatchewan Coldwater Lab, Canmore, Alberta, Canada*

17 Marianne Pietschnig

18 *Department of Mathematics, University of Exeter, Exeter, United Kingdom*

19 Sarah Ragen

20 *School of Oceanography, University of Washington, Seattle, WA, USA*

21 Timothy A. Smith

22 *Oden Institute for Computational Engineering and Sciences, The University of Texas at Austin,*
23 *Austin, TX, USA*

24 David S. Battisti

25 *Department of Atmospheric Sciences, University of Washington, Seattle, WA, USA*

26 **Corresponding author address: Marysa M. Laguë, Department of Earth and Planetary Science,*
27 *University of California Berkeley, 307 McCone Hall, Berkeley, CA 94720.*

28 E-mail: mlague@berkeley.edu

ABSTRACT

29 Motivated by the hemispheric asymmetry of land distribution on Earth, we
30 explore the climate of Northland, a highly idealized planet with a Northern
31 Hemisphere continent and a Southern Hemisphere ocean. The climate of
32 Northland can be separated into four distinct regions: the Southern Hemi-
33 sphere ocean, the seasonally wet tropics, the mid-latitude desert, and the
34 Great Northern Swamp. We evaluate how modifying land surface proper-
35 ties on Northland drives changes in temperatures, precipitation patterns, the
36 global energy budget, and atmospheric dynamics. We observe a surprising
37 response to changes in land-surface evaporation, where suppressing terres-
38 trial evaporation in Northland cools both land and ocean. In previous studies,
39 suppressing terrestrial evaporation has been found to lead to local warming
40 by reducing latent cooling of the land surface. However, reduced evaporation
41 can also decrease atmospheric water vapor, reducing the strength of the green-
42 house effect and leading to large-scale cooling. We use a set of idealized cli-
43 mate model simulations to show that suppressing terrestrial evaporation over
44 Northern Hemisphere continents of varying size can lead to either warming
45 or cooling of the land surface, depending on which of these competing effects
46 dominate. We find that a combination of total land area and contiguous con-
47 tinent size controls the balance between local warming from reduced latent
48 heat flux and large-scale cooling from reduced atmospheric water vapor. Fi-
49 nally, we demonstrate how terrestrial heat capacity, albedo, and evaporation
50 all modulate the location of the ITCZ both over the continent and over the
51 ocean.

52 **1. Introduction**

53 The physical properties of the land surface and the ocean differ in several fundamental ways. For
54 instance, land has a much lower heat capacity than ocean (Cess and Goldenberg 1981; North et al.
55 1983; Bonan 2008); land has a higher albedo than ocean (Budyko 1961, 1969; Payne 1972; Bonan
56 2008); the ocean has the ability to move heat laterally (Loft 1918; Richardson 1980; Trenberth
57 and Caron 2001; Ferrari and Ferreira 2011; Forget and Ferreira 2019); and there are large climatic
58 impacts of terrestrial orography (Queney 1948; Eliassen and Palm 1960; Manabe and Terpstra
59 1974; Held et al. 1985; McFarlane 1987). Moreover, land stores and evaporates less water than
60 ocean, and soil and vegetation properties provide resistance to evaporation over land (Manabe
61 1969; Bonan 2008, and references therein). The contrast between physical properties of land and
62 ocean are important controls on atmospheric dynamics, profoundly impacting the climate. The
63 hemispheric asymmetry in land-sea distribution has implications for global climate, including the
64 higher sensitivity of the Northern Hemisphere to increases in anthropogenic greenhouse gases
65 (Manabe et al. 1991; Stouffer et al. 1989). In this study, we focus on how the limited capacity of
66 the land to hold water, its small heat capacity, and its higher albedo alter the climate system.

67 The albedo of different land types is much higher than that of ice-free ocean. Land albedo ranges
68 from 0.05-0.25 (vegetated) to 0.5-0.9 (glaciers and snow) (Wiscombe and Warren 1980; Oke 1987;
69 Bonan 2008). In contrast, the surface albedo of the ice-free ocean is generally less than 0.1 (Jin
70 et al. 2004). The difference in top-of-atmosphere (TOA) albedo between land and ocean is less
71 drastic, with TOA albedo ranging from 0.25 to 0.6 over snow-free land, and 0.1 to 0.5 over ice-free
72 ocean for Earth in the present climate. These higher values result from atmospheric controls on
73 the TOA albedo, via the effects of cloud cover, aerosols, and attenuation (Donohoe and Battisti
74 2011).

75 Additionally, land has a much smaller heat capacity than the ocean, and a limited ability to
76 move energy laterally. Oceans can absorb large amounts of energy (Kuhlbrodt and Gregory 2012;
77 Cheng et al. 2017) and transport energy via ocean currents; there are areas of the ocean that can
78 continually take up energy, while other regions act as a source of energy to the atmosphere (e.g.
79 Marshall and Zanna 2014; Forget and Ferreira 2019). In contrast, energy absorbed at one location
80 on land must be released back to the atmosphere at that same location in the form of upwards
81 longwave radiation, sensible heat, or latent heat (evaporation). While the land can store energy
82 on seasonal timescales, the seasonal storage of heat by the land surface is much smaller than that
83 of the ocean (Marshall and Plumb 2008). The annual mean heat storage of a land surface in
84 equilibrium is near-zero (Budyko 1974; Milly and Shmakin 2002).

85 The limited capacity of the land surface to hold water and the increased resistance to evapo-
86 ration over land surfaces compared to over open water drastically alters evaporative fluxes over
87 land. Over the ocean, evaporation is determined mainly by the meteorological conditions at the
88 atmosphere-ocean interface (e.g. the surface temperature and atmospheric humidity). In contrast,
89 dry land surfaces have little water available for evaporation, and thus little evaporation occurs re-
90 gardless of the evaporative demand of the overlying atmosphere. Various properties of soil and
91 vegetation further modulate the availability of water to the atmosphere, including total leaf area
92 and roots that can provide access to water deep in the soil column (Canadell et al. 1996; Bonan
93 2008). Moreover, plants directly regulate the movement of water from the land to the atmosphere
94 by opening and closing their stomata (small pores on leaves which modulate gas exchange) (Sellers
95 et al. 1996).

96 These fundamental physical differences between land and ocean result in very different surface-
97 atmosphere interactions. Changes in land surface properties can modify the global climate system
98 (Charney 1975; Shukla and Mintz 1982; Sud et al. 1988; Davin et al. 2010; Laguë et al. 2019).

99 Large hemispheric energy imbalances, such as those generated by sea ice, large-scale vegetation
100 change, or an idealized energy source can drive large-scale changes in the location of the zonal
101 mean Intertropical Convergence Zone (ITCZ) and the Hadley circulation (Chiang and Bitz 2005;
102 Broccoli et al. 2006; Kang et al. 2008; Swann et al. 2012; Laguë and Swann 2016; Kang 2020).
103 In response to a hemispheric energy imbalance, the rising branch of the Hadley circulation moves
104 towards the energy-rich hemisphere, thereby moving energy towards the energy-poor hemisphere
105 and shifting the ITCZ towards the energy-rich hemisphere (Donohoe et al. 2013), provided there
106 are no large changes in gross moist stability (see Geen et al. 2020, and references therein). The
107 distribution of land impacts climate in myriad ways, including by directing storm tracks, shap-
108 ing ocean circulation, generating planetary waves, and impacting orographic forcing and diabatic
109 heating of the atmosphere (Eliassen and Palm 1960; Hartmann 1994; Donohoe et al. 2020).

110 At present, 68% of land on Earth is in the NH and 32% is in the SH. The hemispheric asymmetry
111 in this distribution of land has long been thought to drive asymmetries in surface temperature
112 (Croll 1870; Stouffer et al. 1989; Manabe et al. 1991), precipitation and ocean heat transport
113 (Nilsson et al. 2013). In this study we investigate the climatic implications of the asymmetry
114 in the distribution of land between the Southern Hemisphere (SH) and the Northern Hemisphere
115 (NH). We use an atmospheric general circulation model configuration to explore how fundamental
116 differences between the land and ocean affect the climate. We model the climate of a hypothetical
117 planet that is Earth-like in size and orbital configuration, but has an idealized continent covering the
118 entire Northern Hemisphere, and an ocean covering the entire Southern Hemisphere. We explore
119 the mean state of this planet, which we call Northland, and probe how modifying the albedo of the
120 land surface and its capacity to hold water alter the planet's climate. We also explore the climate
121 of several alternative continental configurations, and consider a land-covered planet.

122 Idealized models are a useful tool in climate science as they help to narrow the gap between
123 simulating the climate system and understanding its mechanisms, as highlighted in Sellers (1969),
124 Held (2005), Jeevanjee et al. (2017), and Maher et al. (2019). Idealized models can be traced back
125 to ‘Galilean’ idealizations, in which a problem is simplified to make it easier to solve (McMullin
126 1985). While an idealized model sacrifices realistic representations of physical processes, this
127 approach aides in illuminating fundamental processes of the climate system (Levins 1966) – in
128 this case, differences between land and ocean surface interactions with the atmosphere.

129 **2. Methods**

130 *a. Model*

131 We use Isca (Vallis et al. 2018), a framework for designing idealized atmospheric general circu-
132 lation models (GCMs), to explore the climate of an Earth-like planet with an idealized continental
133 configuration. The atmosphere is coupled to a 20m slab ocean without any ocean heat transport
134 in our simulations. Land gridcells differ from ocean gridcells by having a higher albedo, smaller
135 heat capacity, a finite reservoir of water, and a parameterized representation of soil moisture that
136 leads to a reduction in evaporation when the soil is less than saturated. The land parameterization
137 used in this study is similar to that of Manabe (1969), where land hydrology is represented using
138 a bucket model. In this model configuration, there is no snow or sea ice, thus no representation
139 of surface albedo feedbacks which would amplify cooling when surface temperatures drop below
140 freezing; soil moisture does not impact land surface albedo.

141 The atmosphere uses moist dynamics, but does not represent clouds. While cloud responses to
142 land surface properties and their changes can play an important role in determining impacts on
143 surface climate (Cho et al. 2018; Sikma and Vilà-Guerau de Arellano 2019; Laguë et al. 2019;

144 Kim et al. 2020), cloud responses to climate perturbations are also a large source of uncertainty
145 (Stocker et al. 2013; Zelinka et al. 2017). Our idealized modeling framework avoids uncertainties
146 associated with cloud responses to climate perturbations, at the cost of not capturing any cloud
147 interaction effects. The surface albedo α of both water ($\alpha_{ocean} = 0.25$) and land ($\alpha_{land} = 0.325$;
148 table 1) is higher than it would be in a model that included clouds, to allow for a more realistic
149 planetary albedo at the top of the atmosphere (Donohoe and Battisti 2011). Despite the absence
150 of clouds, the model still produces precipitation (see Vallis et al. 2018, for details). Simulations
151 are run using a T42 horizontal resolution (roughly 2.8° latitude by 2.8° longitude) with 40 vertical
152 levels.

153 *b. Experiments*

154 We run a total of 14 simulations, with six continental configurations and various land surface
155 properties modified between simulations (table 1). In all simulations, there is a seasonal cycle in
156 insolation (obliquity = 23.439 degrees, eccentricity = 0) with a 360 day year; atmospheric CO₂
157 concentrations are fixed at 300 ppm. We refer to the six continental configurations as “North-
158 land”, “ThreeQuarterLand”, “NorthWestLand”, “ThreePatchLand”, “TwoPatchLand”, and “Lake-
159 world”, (figure 1). Lakeworld is entirely land with no ocean, while TwoPatchLand, ThreePatch-
160 Land, NorthWestLand, ThreeQuarterLand, and Northland have a SH ocean and land covering
161 between half and all of the NH (see table 1 and figure 1 for details).

162 For the Northland continental configuration, we consider 4 simulations with varied land surface
163 properties; we refer to these simulations as “NorthlandXX” (where “XX” indicates a specific
164 simulation). Our “control” simulation (to which we generally compare our other experiments) is
165 “NorthlandBright”. In NorthlandBright, the NH continent has an albedo that is 1.3 times that of
166 the ocean ($\alpha_{land} = 0.325$, $\alpha_{ocean} = 0.25$). The heat capacity of the land is 1/10 that of the ocean in

167 our simulations (i.e. equivalent to a 2m mixed layer ocean). This is larger than the heat capacity of
168 land on Earth, but Isca simulations with realistic continents have been shown to compare well with
169 reanalyses when these heat capacities are used (Thomson and Vallis 2019; Geen et al. 2018). The
170 roughness length is 0.2 mm, and is uniform over land and ocean in our simulations. Hydrology
171 is represented by the “bucket model” (Manabe 1969; Vallis et al. 2018), where the capacity of
172 the land to hold water (“bucket capacity”) is set to 150 mm in our simulations, and water on
173 land is initialized everywhere at 100 mm. The bucket receives water when precipitation exceeds
174 evaporation and loses water when the opposite occurs. When the bucket is more than 3/4 full, the
175 resistance to evaporating water from the land surface is the same as over open water. When the
176 bucket is less than 3/4 full, evaporative resistance scales inversely with the amount of water in the
177 bucket.

178 We run three additional Northland experiments to demonstrate various aspects of the land sur-
179 face’s impact on the climate system. In each of these simulations, a single property of the land
180 surface is modified compared to NorthlandBright. In the “NorthlandDark” experiment, the albedo
181 of the land is reduced so that it is the same as the ocean ($\alpha_{land} = \alpha_{ocean} = 0.25$). In the “North-
182 landEmpty” experiment, the land surface is initialized with no water on the land surface; thus, all
183 water that ends up on land must have originated from the SH ocean. NorthlandEmpty differs from
184 NorthlandBright only in the initial conditions. In the “NorthlandDry” experiment, the capacity
185 of the land to hold water is greatly reduced, to near-zero (0.01 mm). This effectively shuts off
186 evaporation from the land surface.

187 For each of the NorthWestLand, ThreeQuarterLand, TwoPatchLand, and ThreePatchLand con-
188 tinental configurations, we run two simulations. In “NorthWestLand”, “ThreeQuarterLand”,
189 “TwoPatchLand”, and “ThreePatchLand”, the land surface has the same properties as Northland-
190 Bright. In “NorthWestLandDry”, “ThreeQuarterLandDry”, “TwoPatchLandDry”, and “ThreeP-

191 atchLandDry”, the land surface has the same properties as NorthlandDry (i.e. terrestrial evapora-
192 tion is suppressed).

193 We run one simulation where the entire planet is covered with land. We refer to this simulation as
194 “Lakeworld”. Lakeworld has the same albedo as NorthlandBright ($\alpha_{land} = 0.325$), but the bucket
195 hydrology is modified to allow the land to form lakes over gridcells that receive precipitation when
196 the bucket is already full. When the soil moisture is less than 150 mm, the same rules governing
197 terrestrial evaporation in NorthlandBright apply. However, the soil is allowed to accumulate an
198 infinite amount of water. When the soil moisture exceeds 150 mm, the same rules of evaporation
199 for fully saturated soils (which in these simulations are the same as the rules for open water) apply.
200 The lakes do not impact land albedo or heat capacity. Lastly, we run an aquaplanet simulation
201 (“Aqua”) with no land, where the whole planet is covered with a 20m deep mixed layer slab
202 ocean, with an albedo of $\alpha_{ocean} = 0.25$.

203 Most simulations were run for 20 years, though some Northland simulations were run for 50
204 years to check model drift, and Lakeworld was run for 80 years due to the unique water cycle of
205 the all-land planet. The first four years of each simulation are discarded to allow for model spin-
206 up, after which time there is a global-mean drift in surface temperatures of less than 0.01 K/year
207 in the Northland and Aqua simulations (figure S1). Unless otherwise stated, the results presented
208 here are taken from years 5-20 of the simulations (5-80 for Lakeworld). The Lakeworld simulation
209 does not reach equilibrium in 80 years (figure S1), but this simulation is used to demonstrate the
210 transient migration of water, rather than explored for its equilibrium climate.

211 When statistical significance is shown for a difference between two experiments, a student’s
212 t-test is used, with $p < 0.05$ indicating 95% confidence that the simulations differ significantly.
213 When error bars are used, they represent ± 1 standard deviation. Analysis was conducted using

214 the Python programming language, heavily leveraging the Numpy (Harris et al. 2020) and xarray
215 (Hoyer and Hamman 2017) packages.

216 **3. Results**

217 Here our goal is to explore the factors that control the surface energy and hydrologic budgets of
218 the idealized Northland planet. We begin with an overview of the climatology in the Northland-
219 Bright experiment (section a), which we view as a control simulation. We then investigate how
220 changes in land albedo (section b) and terrestrial evaporation (section c) impact the temperature
221 and water cycle of the planet. Next, we explore the effect of suppressing terrestrial evaporation
222 with alternate configurations that include some ocean in the NH (section d). Finally, we explore
223 the role of moisture transport (section e), and show that the mere presence of a continent causes
224 the ITCZ to extend farther poleward than in a pure aquaplanet setting (section f).

225 *a. NorthlandBright (control simulation) climatology*

226 NorthlandBright can be divided into four distinct climatic zones: the SH ocean, the seasonally
227 wet tropical land belt, the NH mid-latitude desert, and the NH moist high-latitude region. The
228 mean climate of the NorthlandBright simulation reflects a world where the area-weighted annual
229 mean surface temperature over the continent is slightly cooler (277K) than over the ocean (280K)
230 (table S1); this is unlike present-day Earth, where – in the extra-tropics – land regions are generally
231 slightly warmer than ocean regions (Wallace et al. 1995; Sutton et al. 2007). The continent has
232 a much larger seasonal cycle of temperature than the ocean, reflecting its smaller heat capacity
233 (figure 2, table S1). The hottest part of the continent, with temperatures reaching 304K, occurs
234 around 30°N during NH summer, while temperatures near the North Pole plunge to 220K during
235 NH winter (figure 2a). Temperatures and seasonality over the SH ocean are much more moderate,

236 with a hemispherically averaged temperature difference of only 4K between summer and winter,
237 compared to 34K in the NH (table S1).

238 The globally averaged annual mean rainfall in the NorthlandBright simulation is approximately
239 2 mm/day. Unsurprisingly, more of this rain falls over the ocean (2.9 mm/day) than over the
240 continent (1.5 mm/day), with a strong latitudinal dependence (figure 2b). The ITCZ has a strong
241 seasonal cycle, with heavier rainfall and a peak that extends farther polewards over the ocean than
242 over the continent (figure 2b, 3a). Over the continent, the ITCZ reaches its farthest poleward
243 extent during August and September, with the peak in precipitation reaching approximately 15°N.
244 In contrast, the peak in the ITCZ over the ocean occurs at around 20°S during March, with roughly
245 double the rate of precipitation in the ocean ITCZ-peak than the land ITCZ-peak. The land cannot
246 support as strong an ITCZ because much of the moisture for the ITCZ must initially be brought
247 onto the land each season by ITCZ precipitation; in contrast, the ocean provides an unlimited
248 supply of water in the form of local evaporation that can subsequently be precipitated in the SH
249 ITCZ.

250 Terrestrial tropical precipitation is most intense from August to November. The land water evap-
251 orates quickly in the tropics due to high insolation (i.e. evaporation has a similar seasonal cycle to
252 precipitation; figure 3a-c). North of 20°N, precipitation is roughly equal to evaporation in the an-
253 nual mean (not shown). Despite heavy wet-season precipitation in the tropics, the ground between
254 0-20°N dries out during the dry season (February-June), because of strong seasonal evaporation
255 (figure 3b,d).

256 In the subtropics of the land hemisphere (roughly 20-40°N) there is a desert with dry soil year-
257 round (figures 2b, 3d). Extratropical precipitation in the land hemisphere features a broad maxi-
258 mum in NH summer that extends from 50°N to the pole that is likely due to localized convection
259 (figure 2b). In the ocean hemisphere, the extratropical maximum in precipitation is located at about

260 40°S, and is storm track precipitation associated with baroclinic cyclones (figure 2b). Precipitation
261 in the ocean hemisphere storm track is nearly seasonally invariant.

262 The high latitude soil is saturated or nearly saturated with water year-round, forming what we
263 call the “Great Northern Swamp” (figure 3d), with slightly less terrestrial water storage during
264 June-July when evaporation (fueled by increased summer insolation) exceeds precipitation (figure
265 3c-d). Interestingly, the soil moisture in the Great Northern Swamp is supplied by water transport
266 from the tropics, and not from local moisture recycling alone. This becomes clear when the land
267 is initialized without any water (NorthlandEmpty). In this simulation, the high latitude soil water
268 is indistinguishable from NorthlandBright within 4-5 years (figures 3d-e). The transport of water
269 to the poles is explored further in section 3e.

270 *b. Climate impacts of land albedo*

271 As we would expect, reducing the albedo of the land surface (making the land darker) leads to
272 surface warming. In NorthlandDark, the land albedo is the same as that of the ocean. As such,
273 the land hemisphere absorbs more solar energy in NorthlandDark than in NorthlandBright (figure
274 S2b), leading to greater temperatures year-round (figure 2c). The additional shortwave (SW) ra-
275 diation absorbed in NorthlandDark compared to NorthlandBright is released to the atmosphere in
276 the form of longwave (LW) radiation, sensible heat or latent heat (figure S2c-f). Increased temper-
277 atures and increased water vapor (resulting in similar relative humidity over the continent between
278 NorthlandDark and NorthlandBright, figure 2e) lead to more downwelling longwave radiation at
279 the surface (figure S2a). That is, the warming in NorthlandDark is due to increased SW absorption
280 as well as increased downwelling LW at the surface. NorthlandDark is warmer than Northland-
281 Bright over both land (+7.4K, figure 2c, table S1) and ocean (+2.4K, figure 2c, table S1), due to
282 atmospheric transport of water vapor and heat. The continent in NorthlandDark is not only warmer

283 than NorthlandBright – it is also wetter, particularly during the months of August-October, when
284 the ITCZ is shifted to the north in NorthlandDark vs. NorthlandBright (figure 2d, figure 4a-b).

285 *c. Climate impacts of reduced terrestrial evaporation*

286 NorthlandDry is the same world as NorthlandBright, except evaporation from the land surface
287 is suppressed. With all else held equal (i.e. the same amount of incoming energy to the land
288 surface, etc.), this reduction in evaporation from the land surface is expected to lead to greater
289 surface temperatures. This is because if evaporative cooling is reduced, the energy absorbed by
290 the surface must be emitted in the form of sensible heat or longwave radiation, both of which
291 require an increase in surface temperatures. Indeed, both Shukla and Mintz (1982) and Laguë
292 et al. (2019) find that reducing evaporation from the land surface leads to surface warming over
293 land.

294 Contrary to previous studies, we find that suppressing evaporation over Northland leads to
295 cooler, not warmer, surface temperatures. Annual mean temperatures in NorthlandDry are 3.2K
296 cooler globally, and 4.9K cooler over land than NorthlandBright (figure 2c, table S1). The cold
297 anomaly is fairly homogeneous over the ocean hemisphere, but is at its greatest during JJA in the
298 northern subtropics (figure 2c). This is surprising as the latent heat flux over land is greatly re-
299 duced in NorthlandDry compared to NorthlandBright (figure 5e), which we would expect to lead
300 to warming. However, suppressing terrestrial evaporation also reduces the amount of water vapor
301 released to the atmosphere over terrestrial regions. Water vapor is a strong greenhouse gas, and if
302 atmospheric water vapor is depleted in sufficiently large quantities, the reduction in the amount of
303 longwave radiation absorbed by the atmosphere and re-emitted down towards the surface would
304 cause net cooling. Moreover, while the direct warming effect of reducing latent cooling is locally
305 isolated to the region where evaporation is reduced, the cooling associated with reduced atmo-

306 spheric water vapor is much broader in spatial extent, as the atmosphere can mix water vapor (or
307 air with reduced water vapor) beyond the locations where terrestrial evaporation was reduced.

308 The decrease in atmospheric water vapor (figure 2f) due to reduced evaporation from the land
309 surface cools NorthlandDry relative to NorthlandBright by reducing downwelling longwave radi-
310 ation (figure 5a). This reduction in downwelling longwave radiation greatly exceeds the reduction
311 in latent heat flux (which on its own would lead to warming). The reduction in downwelling long-
312 wave radiation reaches 150 W/m^2 in the northern high latitudes, while the reduction in latent heat
313 flux peaks at around 80 W/m^2 , with the largest reductions in the northern tropics and high latitudes
314 (compare figure 5a with 5e). In the dry subtropics, the latent heat flux is already near-zero for most
315 of the year in NorthlandBright, so suppressing evaporation has little impact on temperature in this
316 region (figure 5e). Hence, cooling is strongest in the dry subtropics, particularly during JJA (figure
317 2c), because the cooling due to the reduction in downwelling longwave from reduced atmospheric
318 water vapor has no warming offset from local reductions in latent cooling. There is actually a
319 slight increase in net shortwave radiation absorption at the surface over land during NH summer
320 months due to reduced absorption of shortwave radiation by water vapor (figure 5b). However, the
321 decrease in the downwards emission of longwave radiation from reduced atmospheric water vapor
322 dominates the change in absorbed surface energy (figure 5f).

323 At the TOA, there is a substantial reduction in net energy absorbed over the continent from June-
324 August, and an increase in net energy absorbed at the TOA over the continent from September-
325 December (figure 6c). These changes are dominated by the change in TOA LW. During NH
326 summer, more LW is lost from the TOA as a result of a smaller greenhouse effect, and there is
327 less net SW absorption due to reduced atmospheric water vapor (figure 6). That is, despite the
328 surface being colder during JJA in NorthlandDry than NorthlandBright, there is still more LW lost
329 from the TOA in NorthlandDry because of the reduced greenhouse effect. This contrasts with the

330 driver of changes in TOA LW from September-December, when there is overall more energy ab-
331 sorbed at the TOA in NorthlandDry than NorthlandBright (figure 6c). From September-December,
332 NorthlandDry has less LW emission from the TOA, reflecting the overall colder conditions in
333 NorthlandDry compared to NorthlandBright (figure 6b).

334 We can compare the change in land surface temperature over Northland due to suppressed terres-
335 trial evaporation to an equivalent change in albedo, if we assume land surface temperatures scale
336 linearly with land surface albedo (as was found in Laguë et al. (2019)). The surface temperature
337 change between NorthlandDark and NorthlandBright implies a 9.9K increase in land surface tem-
338 peratures per 0.1 decrease in land surface albedo for our idealized planet (see table S1). We note
339 that this is much larger than the roughly 2K increase in surface temperatures per 0.1 decrease in
340 land surface albedo found in Laguë et al. (2019), for a realistic continental configuration in a more
341 complex model. However, intuitively this value should vary with total land area, land distribution,
342 and cloud cover (which is not represented in this model), as modifying land albedo will have a
343 different impact on absorbed SW energy and surface temperatures depending on the presence of
344 clouds and the location of the albedo change. Moreover, surface albedo changes are largely atten-
345 uated by the atmosphere on Earth and in more complex models (Donohoe and Battisti 2011); as
346 such, the 0.1 change in surface albedo between NorthlandBright and NorthlandDark results in a
347 much larger change in planetary albedo in Isca than a similar surface albedo change on the real
348 Earth. Applying the 9.9K/0.1 decrease in albedo relationship for Northland to the temperature
349 change in NorthlandDry vs. NorthlandBright tells us that suppressing terrestrial evaporation over
350 Northland has the equivalent effect on land surface temperatures as increasing the NH albedo by
351 0.05 (roughly 14%, 0.05/0.35).

352 The response of precipitation to suppressed terrestrial evaporation in the NorthlandDry experi-
353 ment is widespread. In particular, precipitation over the continent decreases almost to zero during

354 August-October, which is the wettest part of the year in NorthlandBright. A very weak ITCZ gen-
355 erates a small amount of precipitation over the southern edge of the continent in August-October
356 (figure 4c), while precipitation is very low over the rest of the continent year round. We note
357 that the structure of the Hadley cell during JJA in NorthlandDry differs from the Hadley cell of
358 the other simulations presented here (figure S3). NorthlandDry does not have a large source of
359 moisture over the land surface in the tropics. The ITCZ is very weak during JJA (figure 4c), and
360 rather than an overturning circulation driven by the release of latent heat, the circulation is driven
361 by direct thermal heating of the surface. The result is two overturning cells stacked on the equator
362 during JJA, with the lower cell circulating anti-clockwise and the upper cell circulating clockwise
363 (figure S3f).

364 *d. Temperature response to suppressed evaporation in various continental configurations*

365 The unexpected cooling of Northland with suppressed terrestrial evaporation is due to the re-
366 duction in downwards LW from reduced atmospheric water vapor (and thus a weaker greenhouse
367 effect) dominating any surface warming from reduced latent heat fluxes. Because the Northland
368 continental configuration has no oceanic water source in the NH, NH atmospheric water vapor
369 becomes significantly depleted (figure 7o). We further explore the effects of suppressing terres-
370 trial evaporation on surface temperature by considering four additional continental configurations
371 with varying amounts of ocean in the NH: TwoPatchLand, ThreePatchLand, NorthWestLand, and
372 ThreeQuarterLand (figure 1, table 1). We compare simulations where the continents have the same
373 land surface properties as NorthlandBright (i.e. “normal” land surface properties) to simulations
374 where the continents have the same land surface properties as NorthlandDry (i.e. terrestrial evap-
375 oration is suppressed), to explore the trade-off between warming from reduced surface latent heat
376 flux and cooling from reduced atmospheric water vapor.

377 In TwoPatchLand, suppressing terrestrial evaporation leads to 1.0K of warming over land, on
378 average (figure 7a, 8a). However, as with the dry regions of NorthlandBright, suppressing evap-
379 oration over regions that are climatologically dry in TwoPatchLand (i.e. the subtropics) does not
380 lead to any direct warming through reduced evaporative cooling (figure 7a). Instead, these sub-
381 tropical land areas experience cooling when terrestrial evaporation is suppressed as a result of
382 decreased downwards LW from reduced atmospheric water vapor. In NorthWestLand, suppress-
383 ing evaporation also generally leads to warming over land, with an average warming of 0.7K over
384 land (figures 7b, 8a). The warming is not as strong in NorthWestLand as in TwoPatchLand when
385 evaporation is suppressed (figure 7a), despite both continental configurations having the same to-
386 tal land area and the same latitudinal distribution of land area, with 1/2 of the NH covered by
387 land. The warming is smaller in NorthWestLand despite a comparable (indeed, slightly smaller)
388 reduction in terrestrial latent heat flux (figure 8b).

389 ThreePatchLand and ThreeQuarterLand have the same total land area: in both cases 3/4 of the
390 NH are covered by land. However, suppressing terrestrial evaporation leads to warming of the land
391 for ThreePatchLand, and cooling of the land for ThreeQuarterLand (figure 8a). The warming of
392 0.3K over land in ThreePatchLand is smaller than in TwoPatchLand or NorthWestLand, reflecting
393 the larger reduction in atmospheric water vapor (figure 7i) driven by more land area. In Three-
394 QuarterLand, the reduction in atmospheric water vapor is large enough to dominate warming from
395 reduced latent heat flux, resulting in net land cooling of 0.3K (figures 7j,l, 8a). The reduction in
396 latent heat flux from land is larger in ThreePatchLand than ThreeQuarterLand, but the reduction in
397 latent heat flux from the ocean is much larger in ThreeQuarterLand than in ThreePatchLand (fig-
398 ure 8b). The differences between ThreePatchLand and ThreeQuarterLand (and TwoPatchLand and
399 NorthWestLand) demonstrate that it is not only land area, but also continent size and distribution
400 that modulates the temperature response to suppressed terrestrial evaporation.

401 The change in terrestrial latent heat flux due to suppressed evaporation over land (figure 8b) is
402 approximately equal to the latent heat flux from the simulations with “normal” surface properties
403 (from NorthlandBright), because there is almost no evaporation in the simulations with North-
404 landDry land surface properties. The single large continents have slightly lower latent heat fluxes
405 in the “normal” simulations than their patchy counterparts; that is, TwoPatchLand and ThreePatch-
406 Land have slightly larger terrestrial latent heat fluxes than NorthWestLand and ThreeQuarterLand,
407 respectively, and thus have slightly larger changes in latent heat flux from land when terrestrial
408 evaporation is suppressed.

409 However, we note that the average area-weighted change in latent heat flux from the land surface
410 is of comparable magnitude across all the continental configurations considered here (figure 8b),
411 while total reduction in terrestrial latent heat flux scales with total land area. For simulations with
412 the same total land area (e.g. TwoPatchLand and NorthWestLand), the total reduction in terrestrial
413 latent heat flux is similar, but the surface temperature response differs. The temperature change
414 driven by suppressing terrestrial evaporation is greater when the contiguous continental area is
415 larger. This occurs because the atmosphere becomes more depleted in water vapor over a single
416 large continent than it does over two smaller continents separated by ocean. Thus the water vapor
417 cooling effect is stronger over larger continents than smaller ones, even if the direct warming due
418 to reduced latent cooling of the surface is similar.

419 Over the oceans, surface temperatures cool and evaporation is reduced as a result of suppressing
420 terrestrial evaporation in all the TwoPatchLand, ThreePatchLand, NorthWestLand, ThreeQuarter-
421 Land, and Northland continental configurations (figure 7). The changes in latent heat flux from
422 the ocean (blue bars in figure 8b) must be the result of changes in the local oceanic surface energy
423 budget, mainly over the NH ocean. For example, cooling over the NH ocean in ThreeQuarterLand
424 is more intense than it is over the NH ocean in ThreePatchLand (figure 7 g vs j), which is consis-

425 tent with a greater reduction in oceanic latent heat flux in ThreeQuarterLand vs. ThreePatchLand.
426 Despite Northland showing the greatest surface cooling and the greatest global reduction in latent
427 heat flux, the reduction in oceanic latent heat flux in Northland is small compared to the other
428 continental configurations (figure 8b). This reflects the fact that most of the temperature change
429 in Northland occurs over the land hemisphere, and not over the ocean. In the other continental
430 configurations, much of the reduction in oceanic latent heat flux occurs over the NH, where the
431 temperature changes and decreases in atmospheric water vapor are greatest (figure 7). The cooling
432 over the ocean is due to a reduction in atmospheric water vapor from suppressed terrestrial evapo-
433 ration leading to reductions in downward LW. In turn, cooling over the ocean reduces evaporation
434 from the ocean due to the Clausius Clapeyron relationship. This generates a weak negative feed-
435 back on the ocean temperature, but also further reduces the water vapor flux to the atmosphere.
436 Only in a few ocean regions do we see a slight increase in evaporation (not shown), as might be
437 expected if drier air was being advected off the continent. However, these regions are not all lo-
438 cated downstream of the continents; most of the ocean shows a decrease in evaporation due to a
439 reduced greenhouse effect.

440 We can also consider differences between NorthlandDark and Aqua, as the NH in Northland-
441 Dark has the same albedo as Aqua but a limited capacity to hold water. On the one hand, one
442 might expect the NH land surface in NorthlandDark to be warmer than in Aqua because of limited
443 water available for evaporation (thus potentially less latent cooling of the surface). On the other
444 hand, reduced atmospheric water vapor in the NH of NorthlandDark compared to Aqua could re-
445 sult in cooling (due to a weaker greenhouse effect). In the comparison of NorthlandDark to Aqua
446 however, we are not simply considering differences in water availability; the different NH heat
447 capacities in NorthlandDark and Aqua also lead to differences in evaporation and surface temper-
448 atures. The smaller heat capacity over the land surface in NorthlandDark results in a much larger

449 seasonal cycle in surface temperatures, with hotter summers and cooler winters (figure 9d). The
450 difference in heat capacity also generates big differences in NH evaporation between Northland-
451 Dark and Aqua, since the available energy at the surface in NorthlandDark is used not only to heat
452 the surface, but also to evaporate water (figure 9b,e). In NH summer, high surface temperatures
453 cause a high vapor pressure deficit. Combined with the low heat capacity that requires more en-
454 ergy to be lost by the land surface as heat or moisture, this drives larger latent heat fluxes from the
455 high latitude land in NorthlandDark than in Aqua, despite Aqua having effectively unlimited water
456 to evaporate. Moreover, the larger seasonal cycle in temperature in NorthlandDark vs. Aqua has a
457 non-linear effect on evaporation; the atmospheric demand for water vapor increases exponentially
458 with temperature following the Clausius-Clapeyron relationship such that at the same relative hu-
459 midity the vapor pressure deficit of warmer air is larger than that of cooler air (Hartmann 1994;
460 Bonan 2016). In the annual mean, the tropics in NorthlandDark are hotter and have lower latent
461 heat fluxes than Aqua, while in the high latitudes, surface temperatures are lower and evaporative
462 fluxes are higher. This results in an atmosphere that is drier over the NH in the low latitudes, but
463 actually less dry over the NH high latitudes in NorthlandDark than Aqua (figure 9c). This is no-
464 tably different from the TwoPatchLand, ThreePatchLand, NorthWestLand, and ThreeQuarterLand
465 simulations, but is driven primarily by differences in the heat capacity of land vs. ocean, rather
466 than differences in water availability/evaporation.

467 In summary, we find that suppressing terrestrial evaporation has a direct local warming effect
468 on the region of evaporative suppression, by reducing latent cooling of the land surface. However,
469 suppressing terrestrial evaporation indirectly cools globally by reducing atmospheric water vapor
470 (a strong greenhouse gas). In the case of TwoPatchLand, NorthWestLand, and ThreePatchLand,
471 the local warming effect dominates the response in most terrestrial regions, while the dominant
472 effect over ocean and desert land regions is cooling associated with decreased atmospheric water

473 vapor (figure 8a). However, when evaporation is suppressed over ThreeQuarterLand and North-
474 land, the atmospheric water vapor effect dominates resulting in cooler surface temperatures over
475 the oceans and most land areas (figure 8a). Because Northland does not have any ocean in the
476 Northern Hemisphere, the atmosphere can become much more depleted in water vapor than it
477 can in the other continental configurations (figure 7o). In TwoPatchLand, NorthWestLand, and
478 ThreePatchLand, atmospheric water vapor is depleted over the continents, but is replenished over
479 the ocean at all latitudes, such that the zonal-mean reduction in atmospheric water vapor is much
480 less than the water vapor reduction in Northland (figure 7, right column). While the reduction in
481 atmospheric water vapor isn't as large in ThreeQuarterLand as in Northland, it is large enough for
482 the mean response of land temperatures to be an overall cooling (figures 7j, 8a). We deduce that
483 the land surface temperature response to reduced terrestrial evaporation is a function of both total
484 land area (which controls the reduction in terrestrial latent heat flux) and contiguous continent size
485 (which controls how dry the atmosphere becomes).

486 *e. The role of moisture transport*

487 In all the Northland simulations except NorthlandDry (which can't store water on land), a Great
488 Northern Swamp forms in the northern high latitudes. In the absence of a large low-latitude water
489 source, is the Great Northern Swamp sustainable? Here we use an all-land simulation, Lakeworld,
490 to show that the existence of the Great Northern Swamp relies on atmospheric moisture transport
491 from the SH ocean in all other Northland experiments. Lakeworld has no ocean; land surface
492 properties are similar to those in NorthlandBright except that lakes of arbitrary depth are allowed
493 to form on all gridcells, if precipitation exceeds evaporation.

494 Lakeworld rapidly forms two lakes, one over each pole (figure 3f), which deepen as the simu-
495 lation progresses. Within a few years, all of the water on Lakeworld - which is initialized with

496 100mm of water in every gridcell - has been transported to the polar high latitudes, and the land
497 in the tropics is completely dry year-round. The lake edges retreat polewards quickly over the first
498 35 years, then more slowly as the simulation progresses.

499 In effect atmospheric circulation redistributes water to concentrate it in the polar regions. On
500 the present-day Earth, the lower branch of the Hadley circulation transports moisture equatorward,
501 but in Lakeworld the moisture is rapidly mixed poleward by mid-latitude eddies, then trapped too
502 far poleward for this mechanism of equatorward transport. The atmosphere of Lakeworld is very
503 dry, with atmospheric moisture isolated to the lower troposphere near the summer pole (figure
504 S4). Because the atmosphere in Lakeworld is so dry, the greenhouse effect is very weak, causing
505 Lakeworld to be much colder than the simulations that include some ocean (figure S1, S5). Surface
506 temperatures in Lakeworld are above the freezing point year round in the lower latitudes, and at
507 higher latitudes during summer (figure S5).

508 The polar lake in Lakeworld has a much smaller latitudinal extent than the Great Northern
509 Swamp in the Northland simulations. In the Northland experiments, the southern portion of the
510 Great Northern Swamp receives moisture (which is ultimately from the SH ocean) from mid-
511 latitude eddies. This does not occur in Lakeworld, because moisture is trapped at the poles after
512 the first few years of the simulation. The lake continues to drift poleward over the course of the
513 Lakeworld simulation. The Lakeworld simulation would have to be run to equilibrium to deter-
514 mine how far poleward the polar lake will retreat. However, we do not continue the Lakeworld
515 simulation beyond 80 years as (a) the extent of the polar lake in equilibrium is not the focus of
516 this study and (b) the atmosphere in an all-land configuration leaks moisture in the current con-
517 figuration of Isca (figure S6). We also explore an all-land simulation that cannot form lakes (i.e.
518 it has the same land surface properties as NorthlandBright). Like Lakeworld, that simulation also

519 quickly transports water to the poles, but because runoff is discarded when soil moisture exceeds
520 the bucket capacity, the simulation rapidly loses water from the system (not shown).

521 *f. Land's influence on ITCZ location*

522 The presence of the Northland continent alters the source of energy to the atmosphere by altering
523 the net surface flux of SW (both through surface albedo and changes in water vapor), altering
524 LW absorption in the atmosphere by modulating atmospheric water vapor, and modifying the
525 seasonal timing of energy absorption and release by the land surface. We find that the ITCZ in
526 both the NH and SH of all Northland experiments extends farther poleward than in Aqua (with
527 the exception of NorthlandDry, which has very little precipitation over land), despite the greater
528 water vapor content in the tropics in Aqua (figures 4, 10e). Less SW is absorbed at the NH surface
529 in NorthlandBright compared to Aqua because of the high land albedo in NorthlandBright (figure
530 10c). Except in the northern high latitudes, the atmosphere in NorthlandBright has less water
531 vapor than the atmosphere in Aqua (figure 10a). NorthlandDark has more water vapor over the
532 NH than Aqua as a result of the higher air temperatures (figure 10b). Though the albedo of the
533 NH in NorthlandDark and Aqua are identical, differences in atmospheric water vapor between
534 the simulations result in changes to the amount of SW reaching the surface (figure 10d). The
535 presence of the NorthlandDark continent also results in an ITCZ extending farther poleward than
536 both Aqua and NorthlandBright in the NH (figure 10e). To explain the ITCZ position as a result of
537 the Northland continent in these experiments, we discuss the differences in the hemispheric energy
538 imbalance between our simulations below.

539 There is an extensive literature exploring how hemispherically asymmetric sources of energy
540 to the atmosphere cause the atmosphere to transport energy from the energy-rich hemisphere to
541 the energy-poor hemisphere, with a corresponding shift in the zonally averaged ITCZ towards the

542 energy-rich hemisphere (Kang et al. 2008; Yoshimori and Broccoli 2008; Fasullo and Trenberth
543 2008; Donohoe et al. 2013; Geen et al. 2020). The relationship between the magnitude of cross-
544 equatorial energy transport and the location of the ITCZ has been explored for the modern Earth
545 system, where the ITCZ shifts 2.4-2.7°S per PW increase in northward cross-equatorial energy
546 transport (Donohoe et al. 2013). In our idealized simulations, we find a marginally steeper rela-
547 tionship than Donohoe et al. (2013), with a 3.4° southward shift in the annual mean ITCZ latitude
548 per PW increase in northward cross-equatorial energy transport (figure 11, S7). Several factors
549 impact this slope, including the gross moist stability of the model and the influence of cloud cover,
550 a mechanism which is absent from our experimental framework (Geen et al. 2020; Voigt et al.
551 2014).

552 The greater poleward extent of the zonally averaged ITCZ location is best explained by com-
553 paring the NorthlandDark and Aqua experiments, since these two configurations have the same
554 surface albedo and differ only in the heat capacity and capacity to store water in the NH. We argue
555 that the primary reason for the greater poleward extent of the ITCZ in the Northland simulations is
556 the difference in heat capacity between the land and ocean hemispheres, which generates greater
557 hemispheric energy imbalances than in Aqua – both seasonally and in the annual mean.

558 The lower heat capacity of the NH in NorthlandDark provides less of a buffer to the atmospheric
559 energy imbalance by storing less energy in the surface relative to Aqua during JJA, and releasing
560 less energy during DJF (compare SFC in figure 12f,h and j,l). During JJA, the ITCZ extends farther
561 poleward over the NH in NorthlandDark than Aqua because the land surface takes up little energy,
562 resulting in a larger atmospheric energy source $F_{net} = TOA - SFC$ in NorthlandDark than Aqua
563 (Geen et al. 2020). During DJF, the ITCZ extends farther poleward over the SH in NorthlandDark
564 than Aqua because the land surface releases little energy, while in Aqua the ocean releases stored
565 energy to the atmosphere; thus, the NH atmosphere is more energy-poor in NorthlandDark than

566 Aqua during DJF. The net effect is that the NH atmospheric energy source is much larger in
567 NorthlandDark than Aqua during JJA, while the NH atmospheric energy source is more negative
568 during DJF in NorthlandDark than Aqua (compare F_{net} in figure 12f,h and j,l, table S2).

569 In the annual mean, NorthlandDark has a hemispheric imbalance in F_{net} , while F_{net} is symmetric
570 about the equator in Aqua (table S2). This hemispheric energy imbalance results in an annual mean
571 transport of energy across the equator from the SH to the NH, consistent with a zonally averaged
572 ITCZ sitting south of the equator (figure 11). Corresponding to this hemispheric atmospheric
573 energy imbalance, the ITCZ in NorthlandDark extends much farther poleward than the ITCZ in
574 Aqua, both seasonally and in the annual mean. In NorthlandBright and NorthlandDry, the ITCZ
575 extends slightly farther south than in NorthlandDark during DJF because the lower surface albedo
576 (NorthlandBright) and lower water vapor (NorthlandDry) reduces the total amount of energy taken
577 up during NH summer and subsequently released in NH winter by the land surface, accentuating
578 the hemispheric imbalance in the atmospheric energy source that already exists as a result of the
579 smaller heat capacity of land vs. ocean (figure 12a,c; table S2). Details of the calculations used
580 for figures 11 and 12 are provided in the supplement.

581 **4. Discussion**

582 *a. Temperature response to suppressed terrestrial evaporation*

583 With all else held equal, reducing evaporation from the land surface should lead to surface warm-
584 ing, as the energy formerly used to evaporate water is instead re-partitioned into sensible heat or
585 emitted longwave radiation. While reducing evaporation from the land surface directly leads to
586 warming (Shukla and Mintz 1982; Laguë et al. 2019), reducing water flux from the land surface
587 also impacts atmospheric concentrations of water vapor, a strong greenhouse gas. Given the com-

588 peting effects of reduced evaporative cooling which would lead to warming, and reduced longwave
589 trapping by atmospheric water vapor which would lead to cooling, we hypothesize that a crossing-
590 point exists in the temperature response to suppressed land evaporation (figure 13). Starting from
591 a state of sufficient atmospheric moisture, reducing evaporation from the land surface should ini-
592 tially lead to surface warming as a result of decreased evaporative cooling of the land surface ((i)
593 in figure 13). However, as atmospheric water vapor concentration decreases, the strength of the
594 atmospheric greenhouse effect also decreases, inducing a cooling effect on the surface; the warm-
595 ing signal from suppressed evaporation competes with the cooling from a reduced greenhouse
596 effect ((ii) in figure 13). Once atmospheric concentrations of water vapor are sufficiently low, the
597 cooling effect from the reduced atmospheric greenhouse effect dominates the surface temperature
598 response ((iii) in figure 13).

599 From our simulations, suppressing evaporation over TwoPatchLand would fit into regime (i),
600 where reduced evaporation warms the land surface. NorthWestLand falls between regimes (i) and
601 (ii), where the direct warming effect of reduced evaporation is weaker than in TwoPatchLand, thus
602 the total warming is more strongly damped by the reduction in atmospheric water vapor. Three-
603 PatchLand and ThreeQuarterLand bracket the crossing-point of the temperature response (regime
604 ii), with ThreePatchLand warming slightly and ThreeQuarterLand cooling slightly. Northland
605 falls firmly into regime (iii), where any direct warming of the surface is more than out-weighed
606 by cooling from reduced atmospheric water vapor. Generally, larger total land areas fall farther to
607 the right on this curve; however, for the same total land area (e.g. TwoPatchLand vs. NorthWest-
608 Land), the continental arrangement with the larger contiguous continent size falls farther to the
609 right. This occurs because when the continents are broken up, the atmosphere can be replenished
610 with water vapor when it passes over the ocean, while in the case of a larger contiguous continent,
611 the atmosphere becomes more depleted in water vapor. We suggest the present-day continental

612 configuration of Earth falls into regime (i), both because the present-day continental configuration
613 of Earth most closely resembles TwoPatchLand (i.e. there is ample ocean at every latitude), and
614 because previous modeling studies (e.g. Shukla and Mintz 1982; Laguë et al. 2019) find that re-
615 ducing terrestrial evaporation leads to surface warming over land. Indeed, the largely zonal flow
616 of the atmosphere would shift any continental configuration with ocean at each latitude towards
617 regime (i), as the mixing of dry continental and moist oceanic air would prevent any individual
618 latitude from becoming overly depleted in water vapor.

619 In our simulations, suppressing terrestrial evaporation in all of our continental configurations
620 leads to cooling over the ocean. This differs from the results of Laguë et al. (2019), who found
621 that reduced evaporation with a realistic present-day continental configuration leads to surface
622 warming over most of the ocean.¹ Differences in the ocean temperature response between Laguë
623 et al. (2019) and this study could be due to nuances in circulation due to the use of realistic
624 continental geometry and orography in that study, as well as different intensities of suppressed
625 terrestrial evaporation. In particular, our idealized Isca simulations do not have any representation
626 of cloud cover, and cloud responses to changes in terrestrial evaporation can have large climate
627 feedbacks (Laguë et al. 2019). Reduced terrestrial evaporation can lead to drying of the boundary
628 layer and a reduction in low cloud cover over land, which in turn increases absorbed SW at the
629 surface and drives warming in water-limited systems, while changes in terrestrial evaporation can
630 also lead to cloud changes over ocean regions (Laguë et al. 2019; Kim et al. 2020). Understanding
631 how the presence of clouds, and the response of clouds to reduced terrestrial evaporation, modify
632 the temperature response to reduced terrestrial evaporation both on land and globally requires
633 future study.

¹The Shukla and Mintz (1982) study does not inform on changes over the ocean because they prescribe a fixed SST.

634 Based on our results from TwoPatchLand/ThreePatchLand versus NorthWest-
635 Land/ThreeQuarterLand (section 3d), we postulate that suppressing terrestrial evaporation
636 in continental configurations with large amounts of arid land (e.g. polar continents) would have a
637 much weaker impact on water vapor than continents with moist climates (e.g. in the tropics), and
638 thus would not generate strong large-scale cooling. We also note that we have tested an extreme
639 level of reduced terrestrial evaporation here. We do not consider the response of temperature to
640 smaller reductions in terrestrial evaporation such as those driven by the closure of plants' stomata
641 in response to increased atmospheric CO₂, which have been shown to generate terrestrial warming
642 across CMIP 5 and 6 models (Zarakas et al. 2020).

643 We have explored the temperature response to suppressing terrestrial evaporation over ideal-
644 ized NH continents; in doing so, we have demonstrated that continental configuration is of ut-
645 most importance in controlling the temperature response to suppressed terrestrial evaporation. We
646 have identified the competing effects of suppressing terrestrial evaporation on surface temperature
647 without any complicating factors driven by cloud responses. These idealized simulations do not
648 represent cloud cover, thus do not capture either how the presence of clouds may modulate the
649 surface temperature response to reduced terrestrial evaporation, or how cloud changes in response
650 to reduced terrestrial evaporation may further influence surface temperatures, both locally over
651 land and over the ocean. Further study is required to identify the seasonality of this response,
652 which continental configurations lead to warming vs. cooling, what level of reduction in continen-
653 tal evaporation is required for warming vs. cooling, and what role clouds play in modulating the
654 temperature response to reduced terrestrial evaporation.

655 *b. Connections to Snowball Earth*

656 Our results raise the question of how past continental configurations and distributions of water
657 and vegetation on those continents may have impacted both terrestrial and global paleoclimate
658 through water vapor feedbacks. What is the distribution of continents that is required such that
659 decreasing evapotranspiration from the land surface leads to a cooling rather than warming? In
660 present-day Earth, the greenhouse effect is due mainly to water vapor, and the source of water
661 vapor is net evaporation in the tropics (equatorward of 35° latitude) which is distributed globally by
662 the atmospheric circulation. In our TwoPatchLand and NorthWestLand continental configurations,
663 suppressing terrestrial evaporation results in global-scale cooling through reduced atmospheric
664 water vapor, though the land surface generally warms due to reduced latent cooling. However,
665 in our Northland continental configuration, the continent covers the entire hemisphere, which
666 severely reduces the evapotranspiration of water vapor poleward of the ITCZ in the NH. Further
667 reducing terrestrial evaporation in the NorthlandDry experiment reduces the greenhouse effect
668 and causes cooling. In this regard, it is illuminating to consider the Snowball Earth events: global
669 glaciations during which ice covered the entire surface of the Earth (Kirschvink 1992; Hoffman
670 et al. 1998). There is evidence for two such events during the Neoproterozoic between 630 and
671 750 million years ago, and one in the early Paleoproterozoic 2.5 billion years ago (Abbot et al.
672 2013; Hoffman et al. 2017), when most of the continental land masses were located in the tropics
673 (see Kump et al. 2004; Worsley and Kidder 1991, and references therein).

674 The Snowball Earth atmosphere is cold and holds little moisture (Voigt et al. 2011; Hoffman
675 et al. 2017). Past work suggests that paleogeographic continental configurations cause a reduction
676 in atmospheric water vapor compared to an aquaplanet without continents, increasing direct heat-
677 ing by decreasing cloud cover (Fiorella and Poulsen 2013). Future work could test the robustness

678 of this result and probe whether past tropical megacontinents were large enough to cause a suffi-
679 cient reduction in tropical water vapor to cool the tropics and contribute to the onset of Snowball
680 events (though the dry atmosphere of Snowball Earth is attributed to the cold temperatures and
681 not vice versa (Voigt et al. 2012; Hoffman et al. 2017)). This reduction in tropical water vapor
682 would cause even greater cooling in the extratropics as a consequence of reduced atmospheric
683 energy transport (Rose et al. 2014). If this occurred, cooling by reduced total tropical evaporation
684 would help explain why Snowball Earth happened. However, reductions in continental precipi-
685 tation would reduce the rate of silicate weathering, thus allowing for greater CO₂ buildup in the
686 atmosphere, which would act against the formation of a Snowball Earth event. In addition, past
687 tropical supercontinent configurations would have had some ocean at each latitude band, more
688 closely resembling our NorthWestLand or ThreeQuarterLand simulations than our Northland sim-
689 ulations. Notably, the NorthWestLand and ThreeQuarterLand configurations bracket the transition
690 from warming to cooling when land evaporation is suppressed, suggesting this process could be
691 relevant for Pangea-like continental configurations, though we have not explored the effect of
692 varying the position (e.g. moving the whole continent to the tropics) of the megacontinent here.

693 We note that our NorthlandDry simulation has a similar JJA Hadley cell structure as Snowball
694 Earth. The lack of moisture on the land surface in NorthlandDry means that over the continent
695 during NH summer, as in Snowball Earth, the Hadley circulation is dominated by dry dynamics
696 and produces a much smaller overturning circulation than in the present climate (Voigt et al. 2012;
697 Voigt 2013).

698 *c. Precipitation*

699 In our Northland simulations, we find that the polewards extent of the ITCZ over the ocean
700 hemisphere is influenced by the existence of the NH continent. Specifically, we find the small

701 heat capacity and lower water vapor concentrations of the NH lead to the ocean hemisphere ITCZ
702 extending much farther polewards than it does in an aquaplanet simulation. This is similar to the
703 findings of Bordoni and Schneider (2008) and Wei and Bordoni (2018): that ITCZs in aquaplanets
704 with shallower slab oceans extend farther polewards due to stronger energy gradients between the
705 summer and winter hemispheres. Our Northland simulations also demonstrate the importance of
706 hemispheric asymmetries in surface heat storage.

707 Previous studies have shown how hemispheric energy imbalances drive shifts in the zonal mean
708 location of the ITCZ (e.g. Chiang and Bitz 2005; Broccoli et al. 2006; Kang et al. 2008; Swann
709 et al. 2012; Maroon et al. 2016). In the current continental configuration on Earth, zonal mean
710 changes are not generally representative of regional precipitation change (Byrne and O’Gorman
711 2015; Kooperman et al. 2018; Atwood et al. 2020). However, given our zonally symmetric conti-
712 nental distribution in Northland, the energy balance framework is a useful tool for understanding
713 the seasonal cycle of circulation and the distribution of precipitation.

714 In Earth’s present day continental configuration, roughly 68% of the total land mass is in the
715 NH while the remaining 32% is in the SH. This work raises the question of how much the present
716 day continental configuration impacts the ITCZ location via asymmetries in seasonal heat storage
717 between the hemispheres.

718 The present study ties into previous work exploring the impact of continental land masses on
719 the climate system. The tropical rain belts with an annual cycle and a continent model intercom-
720 parison project (TRACMIP, Voigt et al. 2016) showed that the presence of an idealised tropical
721 continent spanning 45° in longitude generally leads to a decrease in global-mean surface tem-
722 peratures compared to an aquaplanet in several different GCMs. The authors noted that while
723 this cooling might be expected from the increase in planetary albedo, the patterns of change are
724 more complex and probably related to changes in cloud cover. Voigt et al. (2016) used a “jello-

725 continent”, which is essentially a patch of thin (lower heat capacity) ocean with higher albedo and
726 reduced evaporation. In contrast to our study, there is no limit on water availability for evaporation
727 over the jello-continent, which would be equivalent to unlimited soil moisture in our experiments.
728 Simulations with “jello” continents in an Earth-like configuration generally capture the present-
729 day climate well (Geen et al. 2018; Thomson and Vallis 2019), but might be too idealized for
730 studying precipitation change in response to CO₂ forcing in some tropical regions such as the
731 Amazon basin (Pietschnig et al. 2019). While the reduction in evaporation due to the presence of
732 land leads to cooling in TRACMIP, similar to what we see from Aqua to NorthlandDark or from
733 NorthlandBright to NorthlandDry, the mechanisms for the cooling are different. First, clouds are
734 not modelled in Isca but are noted to have an impact of surface temperature patterns in TRACMIP.
735 Second, the inability of the jello-continent to dry out makes the “warming due to reduced latent
736 cooling” (figure 13 (i)) less extreme, though at the same time the reduction in atmospheric water
737 vapor – which would lead to cooling (figure 13 (iii)) – would be expected to be less drastic than in
738 our study.

739 *d. Relationship to all-land planets*

740 Our Lakeworld simulation rapidly transports all the surface water to the poles. We expect this is
741 because the climatological equator-to-pole temperature gradient ensures an even greater gradient
742 in moisture (via the Clausius-Clapeyron relationship), and atmospheric storms transport water
743 vapor towards the high latitudes where the vapor condenses and precipitates. The condensate
744 remains at the poles because evaporation is greatly reduced by the cooling resulting from the
745 reduced greenhouse effect. During summer, some of the high-latitude soil moisture evaporates, but
746 is locally recycled. In the absence of an efficient mechanism to transport moisture from the poles
747 towards the equator, all the moisture ends up accumulating in the polar regions. This “leaking” of

748 moisture from the tropics to the poles warrants further study: e.g. how much water does the system
749 require to maintain a moist tropics? What controls the latitudinal extent of the polar lake? This
750 distribution of surface water is similar to that on other planets, such as Mars, which has two polar
751 ice caps (Boynton et al. 2002; Wordsworth 2016; Feldman et al. 2004). While the mechanism by
752 which the water on Mars is concentrated in its polar regions is unclear (Wordsworth 2016), we
753 note that this is an intriguing similarity with our all-land simulation.

754 The presence of large topographical features could potentially modify the distribution of water
755 on a land planet, as it could favour the formation of lakes via runoff into basins rather than at the
756 poles. The distribution of the lakes would then be controlled by surface topography rather than
757 atmospheric moisture transport alone, as is the case in our simulations. Indeed, previous studies
758 of all-land planets that include overland river-like mechanisms to bring water back from the high
759 latitudes to the low latitudes have high soil moisture outside of the polar regions and precipitation
760 maxima in the mid latitude storm tracks (e.g. Kalidindi et al. 2018), unlike our Lakeworld simula-
761 tion which has soil moisture maxima at the poles. In their land-planet simulation, Kalidindi et al.
762 (2018) find two distinct climate states in the absence of a seasonal cycle – one hot and dry, and one
763 cold and wet; including a seasonal cycle only produces a cold and wet state. While our all-land
764 simulation is cold and wet near the poles, the absence of surface water redistribution means that
765 the tropics in our Lakeworld simulation are cold (compared to Aqua or Northland) and dry. Dif-
766 ferences between our results and those of Kalidindi et al. (2018) arise from the addition of clouds,
767 zero obliquity, and importantly the resupply of water to low latitudes in their study. We suspect
768 that without the water recycling mechanism and with a seasonal cycle, Kalidindi et al. (2018)
769 would also observe low values of soil moisture and precipitation except very close to the poles.

770 **5. Conclusions**

771 In this study, we use an idealized climate model to study the climate of Northland, a planet
772 with a continent covering the NH and an ocean covering the SH, and several related continental
773 configurations where the NH contains both land and ocean. The physical properties of land on
774 Earth differ from the ocean in several ways, each of which has an effect on the climate system.
775 Land has a limited capacity to hold water, a higher albedo, and a smaller heat capacity than oceans,
776 and evaporation and turbulent energy exchange from the land surface are influenced by properties
777 of vegetation and soils. By conducting a series of simulations where specific properties of the
778 land surface are modified, we test the sensitivity of surface climate and atmospheric circulation to
779 various aspects of the land surface.

780 The climatology of Northland has a seasonal temperature cycle that is greatly amplified over the
781 land hemisphere, due to the limited heat capacity of the land surface. On the continent, the tropics
782 are seasonally wet; moisture is brought onto the continent from the ocean by the land-falling
783 ITCZ, but the soils dry out during NH winter. From 20°N-40°N, there is a desert region. In the
784 high latitudes, soils are moist year round. There is rain over high latitude land during NH summer;
785 in contrast, precipitation declines polewards of 45°S in the ocean hemisphere in all seasons. We
786 show that atmospheric moisture transport forms a swampy region in the high latitudes, both in our
787 Northland simulations and over a land-only planet.

788 Surprisingly, we find that suppressing terrestrial evaporation over the Northland continent leads
789 to global-scale cooling, with particularly large cooling of 4.9K over the NH continent – this is in
790 contrast to previous studies which find reducing terrestrial evaporation warms the land surface.
791 With all else held equal, decreasing evaporation would lead to warming as the land surface would
792 have to shed energy through sensible heat or emitted longwave radiation, both of which are a

793 function of surface temperature. However, in our simulations, we find that suppressing terrestrial
794 evaporation reduces atmospheric water vapor concentrations, and in turn decreases the strength of
795 the greenhouse effect. The decrease in the greenhouse effect due to reduced water vapor leads to
796 surface cooling which outweighs any surface warming resulting directly from reduced evaporative
797 cooling in the Northland continental configuration. Using a series of alternative continental con-
798 figurations where only part of the NH is covered with land, we demonstrate that there is a trade-off
799 between the local warming effect of reduced latent heat flux and the global cooling effect of re-
800 duced atmospheric water vapor. When the NH has two 90° wide continents separated by ocean,
801 suppressing terrestrial evaporation leads to 1K of warming over land, while a single 180° wide NH
802 continent leads to weaker warming of 0.7K over land. Three equally spaced 90° wide NH conti-
803 nents lead to even weaker warming of 0.3K over land, while a single 270° wide continent leads to
804 cooling of 0.3K over land. The land only experiences warming as a result of suppressed terrestrial
805 evaporation in regions with soil moisture (i.e. not in the subtropics). Over the oceans, suppress-
806 ing terrestrial evaporation leads to reduced atmospheric water vapor and decreased downwelling
807 LW, which reduces sea surface temperatures and ocean evaporation, in turn further reducing at-
808 mospheric water vapor. We conclude that both globally and over land, the temperature response
809 to suppressed terrestrial evaporation is not only a function of total land area and the latitudinal
810 distribution of land, but also of continent size.

811 We find that the ITCZ extends much farther polewards, both over the land and ocean hemi-
812 spheres, in our Northland simulations compared to an aquaplanet simulation. This is primarily the
813 result of the difference in surface heat capacity between the land and ocean hemispheres, which
814 leads to a larger hemispheric imbalance in atmospheric energy in the Northland simulations com-
815 pared to an aquaplanet.

816 By exploring the climate of Northland, this study provides insight into the role of hemispheric
817 asymmetries in continental distribution on surface climate and atmospheric circulation, as well as
818 into energetic constraints on the ITCZ location. We have identified a fundamental trade-off in the
819 effect of terrestrial evaporation on surface temperatures which warrants further study. Northland
820 provides an ideal limit for probing fundamental impacts of hemispheric asymmetries and raises
821 new questions about the role of continental distribution, planetary albedo, and terrestrial evapora-
822 tion in modulating the climate system.

823 *Data availability statement.* The Isca climate model is publicly available at <https://github.com/ExeClim/Isca>. The data presented in this paper is archived on Dryad, accessible at <https://datadryad.org/stash/share/k1nIAE1nV4tfbZfbCQ0p49qQp8xv1CyBoF9-c1jCDyU>. We
824 will update this with a public link and doi (<https://doi.org/10.6078/D1399Q>) upon accep-
825 tance of this paper.

828 *Acknowledgments.* We wish to thank the organizers of the 2018 Advanced Climate Dy-
829 namics Course, where this project began ([https://www.uib.no/en/rs/acdc/118773/](https://www.uib.no/en/rs/acdc/118773/acdc-2018-hemispheric-asymmetry-climate)
830 [acdc-2018-hemispheric-asymmetry-climate](https://www.uib.no/en/rs/acdc/118773/acdc-2018-hemispheric-asymmetry-climate)). We thank W. R. Boos, A. L. S. Swann, and
831 W. Kang for their helpful discussions and feedback. We acknowledge postdoctoral funding sup-
832 port for MML from the James S. McDonnell Foundation Postdoctoral Fellowship in Dynamic and
833 Multiscale Systems. MP acknowledges funding by the University of Exeter College of Engineer-
834 ing Mathematics and Physical Sciences, and the UK - China Research and Innovation Partnership
835 Fund through the Met Office Climate Science for Service Partnership (CSSP) China as part of the
836 Newton Fund. In addition, MP's gratitude is due to the Rupert Ford Award (administered by the
837 Royal Meteorological Society) and the University of Exeter College of Engineering Mathematics
838 and Physical Sciences PhD Mobility Fund who provided the funding for her research visit to the

839 University of Washington, Seattle, which facilitated collaboration on this project. We thank the
840 editor and three reviewers for their thoughtful, constructive feedback on this manuscript.

841 **References**

842 Abbot, D. S., A. Voigt, D. Li, G. L. Hir, R. T. Pierrehumbert, M. Branson, D. Pollard, and D. D.
843 B. Koll, 2013: Robust elements of snowball earth atmospheric circulation and oases for life.
844 *Journal of Geophysical Research: Atmospheres*, **118** (12), 6017–6027.

845 Atwood, A. R., A. Donohoe, D. S. Battisti, X. Liu, and F. S. R. Pausata, 2020: Robust
846 longitudinally-variable responses of the ITCZ to a myriad of climate forcings. *Geophysical*
847 *Research Letters*, **47** (17), 1–13, doi:10.1029/2020GL088833.

848 Bonan, G., 2016: *Ecological Climatology*. 3rd ed., Cambridge University Press, doi:10.1017/
849 cbo9781107339200.

850 Bonan, G. B., 2008: *Ecological Climatology*. Cambridge Univ. Press, Cambridge, UK.

851 Bordoni, S., and T. Schneider, 2008: Monsoons as eddy-mediated regime transitions of the tropical
852 overturning circulation. *Nature Geoscience*, **1** (8), 515–519, doi:10.1038/ngeo248.

853 Boynton, W. V., and Coauthors, 2002: Distribution of hydrogen in the near surface of Mars: Evi-
854 dence for subsurface ice deposits. *Science*, **297** (5578), 81–85, doi:10.1126/science.1073722.

855 Broccoli, A. J., K. a. Dahl, and R. J. Stouffer, 2006: Response of the ITCZ to Northern Hemisphere
856 cooling. *Geophysical Research Letters*, **33** (1), 1–4, doi:10.1029/2005GL024546.

857 Budyko, M. I., 1961: The Heat Balance of the Earth's Surface. *Soviet Geography*, **2** (4), 3–13,
858 doi:10.1080/00385417.1961.10770761.

- 859 Budyko, M. I., 1969: The effect of solar radiation variations on the climate of the Earth. *Tellus*,
860 **21 (5)**, 611–619, doi:10.3402/tellusa.v21i5.10109.
- 861 Budyko, M. I., 1974: *Climate and life*. Academic Press, Inc.
- 862 Byrne, M. P., and P. A. O’Gorman, 2015: The response of precipitation minus evapotranspiration
863 to climate warming: Why the ”Wet-get-wetter, dry-get-drier” scaling does not hold over land.
864 *Journal of Climate*, **28 (20)**, 8078–8092, doi:10.1175/JCLI-D-15-0369.1.
- 865 Canadell, A. J., R. B. Jackson, J. R. Ehleringer, H. A. Mooney, O. E. Sala, and E. Schulze, 1996:
866 Maximum Rooting Depth of Vegetation Types at the Global Scale. *Oecologia*, **108 (4)**, 583–595.
- 867 Cess, R. D., and S. D. Goldenberg, 1981: The effect of ocean heat capacity upon global warming
868 due to increasing atmospheric carbon dioxide. *Journal of Geophysical Research*, **86 (80)**, 498–
869 502.
- 870 Charney, J. G., 1975: Dynamics of deserts and drought in the Sahel. *Quarterly Journal of the*
871 *Royal Meteorological Society*, **101 (428)**, 193–202, doi:10.1002/qj.49710142802.
- 872 Cheng, L., K. E. Trenberth, J. Fasullo, T. Boyer, J. Abraham, and J. Zhu, 2017: Improved estimates
873 of ocean heat content from 1960 to 2015. *Science Advances*, **3 (3)**, e1601 545.
- 874 Chiang, J. C. H., and C. M. Bitz, 2005: Influence of high latitude ice cover on the marine Intertrop-
875 ical Convergence Zone. *Climate Dynamics*, **25 (5)**, 477–496, doi:10.1007/s00382-005-0040-5.
- 876 Cho, M. H., A. R. Yang, E. H. Baek, S. M. Kang, S. J. Jeong, J. Y. Kim, and B. M. Kim, 2018:
877 Vegetation-cloud feedbacks to future vegetation changes in the Arctic regions. *Climate Dynam-*
878 *ics*, **50 (9-10)**, 3745–3755, doi:10.1007/s00382-017-3840-5.
- 879 Croll, J., 1870: XII. On ocean-currents. *The London, Edinburgh, and Dublin Philosophical Mag-*
880 *azine and Journal of Science*, **39 (259)**, 81–106.

- 881 Davin, E. L., N. de Noblet-Ducoudré, N. de Noblet-Ducoudre, and N. de Noblet-Ducoudré, 2010:
882 Climatic Impact of Global-Scale Deforestation: Radiative versus Nonradiative Processes. *Jour-*
883 *nal of Climate*, **23** (1), 97–112, doi:10.1175/2009JCLI3102.1.
- 884 Donohoe, A., K. C. Armour, G. H. Roe, D. S. Battisti, and L. Hahn, 2020: The Partitioning of
885 Meridional Heat Transport from the Last Glacial Maximum to CO2 Quadrupling in Coupled
886 Climate Models. *Journal of Climate*, **33** (10), 4141–4165, doi:10.1175/jcli-d-19-0797.1.
- 887 Donohoe, A., and D. S. Battisti, 2011: Atmospheric and surface contributions to planetary albedo.
888 *Journal of Climate*, **24** (16), 4402–4418, doi:10.1175/2011JCLI3946.1.
- 889 Donohoe, A., J. Marshall, D. Ferreira, and D. Mcgee, 2013: The relationship between ITCZ
890 location and cross-equatorial atmospheric heat transport: From the seasonal cycle to the Last
891 Glacial Maximum. *Journal of Climate*, **26** (11), 3597–3618, doi:10.1175/JCLI-D-12-00467.1.
- 892 Eliassen, A., and E. Palm, 1960: On the Transfer of Energy in Stationary Mountain Waves. *Geof-*
893 *ysiske Publikasjoner*.
- 894 Fasullo, J. T., and K. E. Trenberth, 2008: The Annual Cycle of the Energy Budget. Part II:
895 Meridional Structures and Poleward Transports. *Journal of Climate*, **21** (10), 2313–2325, doi:
896 10.1175/2007JCLI1936.1.
- 897 Feldman, W. C., and Coauthors, 2004: Global distribution of near-surface hydrogen on Mars.
898 *Journal of Geophysical Research E: Planets*, doi:10.1029/2003JE002160.
- 899 Ferrari, R., and D. Ferreira, 2011: What processes drive the ocean heat transport? *Ocean Mod-*
900 *elling*, doi:10.1016/j.ocemod.2011.02.013.
- 901 Fiorella, R. P., and C. J. Poulsen, 2013: Dehumidification over tropical continents reduces climate
902 sensitivity and inhibits snowball earth initiation. *Journal of Climate*, **26** (23), 9677–9695.

903 Forget, G., and D. Ferreira, 2019: Global ocean heat transport dominated by heat export from the
904 tropical Pacific. *Nature Geoscience*, doi:10.1038/s41561-019-0333-7.

905 Geen, R., S. Bordoni, D. S. Battisti, and K. Hui, 2020: Monsoons, ITCZs and the Concept of the
906 Global Monsoon. *Reviews of Geophysics*, 1–45, doi:10.1029/2020rg000700.

907 Geen, R., F. H. Lambert, and G. K. Vallis, 2018: Regime Change Behavior during Asian Monsoon
908 Onset. *Journal of Climate*, **31** (8), 3327–3348, doi: 10.1175/JCLI-D-17-0118.1.

909 Harris, C. R., and Coauthors, 2020: Array programming with NumPy. *Nature*, **585** (7825), 357–
910 362, doi:10.1038/s41586-020-2649-2.

911 Hartmann, D. L., 1994: *Global physical climatology*, Vol. 56. Academic press.

912 Held, I. M., 2005: The gap between simulation and understanding in climate modeling. *Bulletin*
913 *of the American Meteorological Society*, **86** (11), 1609–1614.

914 Held, I. M., P. L. Panetta, and R. T. Pierrehumbert, 1985: Stationary external Rossby waves in
915 vertical shear. 865–883 pp., doi:10.1175/1520-0469(1985)042<0865:SERWIV>2.0.CO;2.

916 Hoffman, P. F., A. J. Kaufman, G. P. Halverson, and D. P. Schrag, 1998: A Neoproterozoic Snow-
917 ball Earth. *Science*, **281** (5381), 1342–1346, doi:10.1126/science.281.5381.1342.

918 Hoffman, P. F., and Coauthors, 2017: Snowball Earth climate dynamics and Cryogenian geology-
919 geobiology. *Science Advances*, **3** (11), doi:10.1126/sciadv.1600983.

920 Hoyer, S., and J. Hamman, 2017: xarray: N-D labeled arrays and datasets in Python. *Journal of*
921 *Open Research Software*, **5** (1), doi:10.5334/jors.148.

922 Jeevanjee, N., P. Hassanzadeh, S. Hill, and A. Sheshadri, 2017: A perspective on climate model
923 hierarchies. *Journal of Advances in Modeling Earth Systems*, **9** (4), 1760–1771, doi:10.1002/
924 2017MS001038.

925 Jin, Z., T. P. Charlock, W. L. Smith, and K. Rutledge, 2004: A parameterization of ocean surface
926 albedo. *Geophysical Research Letters*, **31** (22), 1–4, doi:10.1029/2004GL021180.

927 Kalidindi, S., C. H. Reick, T. Raddatz, and M. Claussen, 2018: Two drastically different
928 climate states on an Earth-like terra-planet. *Earth System Dynamics*, **9** (2), 739–756, doi:
929 10.5194/esd-9-739-2018.

930 Kang, S. M., 2020: Extratropical Influence on the Tropical Rainfall Distribution. **1**, 24–36.

931 Kang, S. M., I. M. Held, D. M. W. Frierson, and M. Zhao, 2008: The Response of the ITCZ
932 to Extratropical Thermal Forcing: Idealized Slab-Ocean Experiments with a GCM. *Journal of*
933 *Climate*, **21** (14), 3521–3532, doi:10.1175/2007JCLI2146.1.

934 Kim, J. E., M. M. Laguë, and A. L. S. Swann, 2020: Evaporative Resistance is of Equal Importance
935 as Surface Albedo in High-Latitude Surface Temperatures Due to Cloud Feedbacks. 1–10, doi:
936 10.1029/2019GL085663.

937 Kirschvink, J. L., 1992: Late Proterozoic low-latitude global glaciation: the snowball Earth. *The*
938 *Proterozoic Biosphere*, **52**, 51–52, doi:10.1038/scientificamerican0100-68.

939 Kooperman, G. J., Y. Chen, F. M. Hoffman, C. D. Koven, K. Lindsay, M. S. Pritchard, A. L. S.
940 Swann, and J. T. Randerson, 2018: Forest response to rising CO₂ drives zonally asymmetric
941 rainfall change over tropical land. *Nature Climate Change*, **8**, doi: 10.1038/s41558-018-0144-7.

942 Kuhlbrodt, T., and J. Gregory, 2012: Ocean heat uptake and its consequences for the magnitude of
943 sea level rise and climate change. *Geophysical Research Letters*, **39** (18).

944 Kump, L. R., J. F. Kasting, R. G. Crane, and others, 2004: *The Earth System*, Vol. 432. Pearson
945 Prentice Hall Upper Saddle River, NJ.

946 Laguë, M. M., G. B. Bonan, and A. L. S. Swann, 2019: Separating the Impact of Individual
947 Land Surface Properties on the Terrestrial Surface Energy Budget in both the Coupled and
948 Uncoupled Land–Atmosphere System. *Journal of Climate*, **32 (18)**, 5725–5744, doi:10.1175/
949 jcli-d-18-0812.1.

950 Laguë, M. M., and A. L. Swann, 2016: Progressive midlatitude afforestation: Impacts on clouds,
951 global energy transport, and precipitation. *Journal of Climate*, **29 (15)**, 5561–5573, doi:10.1175/
952 jcli-d-15-0748.1.

953 Levins, R., 1966: The Strategy of Model Building in Population Biology. *American Scientist*,
954 **5 (41)**, 420–431.

955 Loft, G., 1918: The Gulf Stream and the North Atlantic Drift. *Journal of Geography*, **17 (1)**, 8–17,
956 doi:10.1080/00221341808984367.

957 Maher, P., and Coauthors, 2019: Model Hierarchies for Understanding Atmospheric Circulation.
958 doi:10.1029/2018RG000607.

959 Manabe, S., 1969: Climate and the Ocean Circulation. *Monthly Weather Review*, **97 (11)**, 739–
960 774, doi:10.1175/1520-0493(1969)097<0739:CATOC>2.3.CO;2.

961 Manabe, S., R. J. Stouffer, M. J. Spelman, and K. Bryan, 1991: Transient responses of a cou-
962 pled ocean–atmosphere model to gradual changes of atmospheric CO₂. Part I. Annual mean
963 response. *Journal of Climate*, **4 (8)**, 785–818.

964 Manabe, S., and T. B. Terpstra, 1974: The effect of mountains on the general circulation of the
965 Atmosphere. 3 pp.

966 Maroon, E. A., D. M. Frierson, S. M. Kang, and J. Scheff, 2016: The precipitation response
967 to an idealized subtropical continent. *Journal of Climate*, **29** (12), 4543–4564, doi:10.1175/
968 JCLI-D-15-0616.1.

969 Marshall, D. P., and L. Zanna, 2014: A conceptual model of ocean heat uptake under climate
970 change. *Journal of Climate*, **27** (22), 8444–8465.

971 Marshall, J., and R. A. Plumb, 2008: *Atmosphere, ocean, and climate dynamics: an introductory*
972 *text*, Vol. 93. Elsevier Academic Press.

973 McFarlane, N. A., 1987: The Effect of Orographically Excited Gravity Wave Drag on the Gen-
974 eral Circulation of the Lower Stratosphere and Troposphere. 1775–1800 pp., doi:10.1175/
975 1520-0469(1987)044<1775:teooeg>2.0.co;2.

976 McMullin, E., 1985: Galilean idealization. *Studies in History and Philosophy of Science Part A*,
977 **16** (3), 247–273.

978 Milly, P. C. D., and a. B. Shmakin, 2002: Global Modeling of Land Water and Energy Balances.
979 Part I: The Land Dynamics (LaD) Model. *Journal of Hydrometeorology*, **3** (3), 283–299, doi:
980 10.1175/1525-7541(2002)003<0283:GMOLWA>2.0.CO;2.

981 Nilsson, J., P. L. Langen, D. Ferreira, and J. Marshall, 2013: Ocean basin geometry and the
982 salinification of the Atlantic Ocean. *Journal of Climate*, doi:10.1175/JCLI-D-12-00358.1.

983 North, G. R., J. G. Mengel, and D. A. Short, 1983: Simple energy balance model resolving the
984 seasons and the continents: Application to the astronomical theory of the ice ages. *Journal of*
985 *Geophysical Research*, **88** (C11), 6576–6586, doi:10.1029/JC088iC11p06576.

986 Oke, T. R., 1987: *Boundary layer climates, Second edition*. doi:10.1017/CBO9781107415324.
987 004.

- 988 Payne, R. E., 1972: Albedo of the Sea Surface. 959–970 pp., doi:10.1175/1520-0469(1972)
989 029(0959:aotss)2.0.co;2.
- 990 Pietschnig, M., F. H. Lambert, M. Saint-Lu, and G. K. Vallis, 2019: The Presence of Africa and
991 Limited Soil Moisture Contribute to Future Drying of South America. *Geophysical Research
992 Letters*, **46 (21)**, 12 445–12 453, doi:10.1029/2019GL084441.
- 993 Queney, P., 1948: The Problem of Air Flow Over Mountains: A Summary of Theoretical Studies.
994 *Bulletin of the American Meteorological Society*, **29 (1)**, 16–26, doi:10.1175/1520-0477-29.1.
995 16.
- 996 Richardson, P. L., 1980: Benjamin Franklin and Timothy Folger’s First Printed Chart of the Gulf
997 Stream. *Science*, **207 (4431)**, 643–645.
- 998 Rose, B. E. J., K. C. Armour, D. S. Battisti, N. Feldl, and D. D. B. Koll, 2014: The dependence of
999 transient climate sensitivity and radiative feedbacks on the spatial pattern of ocean heat uptake.
1000 *Geophysical Research Letters*, **41 (3)**, 1071–1078.
- 1001 Sellers, P. J., and Coauthors, 1996: Comparison of radiative and physiological effects of dou-
1002 bled atmospheric CO₂ on climate. *SCIENCE-NEW YORK THEN WASHINGTON-*, **271 (5254)**,
1003 1402–1405, doi:10.1126/science.271.5254.1402.
- 1004 Sellers, W. D., 1969: Global Climatic Model Based on the Energy Balance of the Earth-
1005 Atmosphere System. *Journal of Applied Meteorology*, **8 (3)**, 392–400.
- 1006 Shukla, J., and Y. Mintz, 1982: Influence of Land-Surface Evapotranspiration on the Earth’s Cli-
1007 mate. *Science*, **215 (4539)**, 1498–1501.

- 1008 Sikma, M., and J. Vilà-Guerau de Arellano, 2019: Substantial Reductions in Cloud Cover and
1009 Moisture Transport by Dynamic Plant Responses. *Geophysical Research Letters*, **46** (3), 1870–
1010 1878, doi:10.1029/2018GL081236.
- 1011 Stocker, T. F., and Coauthors, 2013: Climate change 2013 the physical science basis: Working
1012 Group I contribution to the fifth assessment report of the Intergovernmental Panel on Climate
1013 Change. *Contribution of Working Group I to the Fifth Assessment Report of the Intergovern-
1014 mental Panel on Climate Change.*, **9781107057**, 1–1535, doi:10.1017/CBO9781107415324.
- 1015 Stouffer, R. J., S. Manabe, and K. Bryan, 1989: Interhemispheric asymmetry in climate response
1016 to a gradual increase of atmospheric CO₂. *Nature*, **342** (6250), 660–662.
- 1017 Sud, Y. C., J. Shukla, and Y. Mintz, 1988: Influence of Land Surface Roughness on Atmospheric
1018 Circulation and Precipitation: A Sensitivity Study with a General Circulation Model. 1036–
1019 1054 pp., doi:10.1175/1520-0450(1988)027<1036:iolsro>2.0.co;2.
- 1020 Sutton, R. T., B. Dong, and J. M. Gregory, 2007: Land/sea warming ratio in response to climate
1021 change: IPCC AR4 model results and comparison with observations. *Geophysical Research
1022 Letters*, **34** (2), 2–6, doi:10.1029/2006GL028164.
- 1023 Swann, A. L. S., I. Y. Fung, and J. C. H. Chiang, 2012: Mid-latitude afforestation shifts general
1024 circulation and tropical precipitation. *Proceedings of the National Academy of Sciences*, **109** (3),
1025 712–716, doi:10.1073/pnas.1116706108.
- 1026 Thomson, S. I., and G. K. Vallis, 2019: Hierarchical Modeling of Solar System Planets with Isca.
1027 *Atmosphere*, **10** (12), 803, doi: 10.3390/atmos10120803.
- 1028 Trenberth, K. E., and J. M. Caron, 2001: Estimates of meridional atmosphere and ocean heat
1029 transports. *Journal of Climate*, **14** (16), 3433–3443.

- 1030 Vallis, G. K., and Coauthors, 2018: Isca, v1.0: A framework for the global modelling of the
1031 atmospheres of Earth and other planets at varying levels of complexity. *Geoscientific Model*
1032 *Development*, **11** (3), 843–859, doi:10.5194/gmd-11-843-2018.
- 1033 Voigt, A., 2013: The dynamics of the Snowball Earth Hadley circulation for off-equatorial
1034 and seasonally varying insolation. *Earth System Dynamics*, **4** (2), 425–438, doi:10.5194/
1035 esd-4-425-2013.
- 1036 Voigt, A., D. Abbot, R. Pierrehumbert, and J. Marotzke, 2011: Initiation of a marinoan snowball
1037 earth in a state-of-the-art atmosphere-ocean general circulation model. *Climate of the Past*, **7**,
1038 249–263.
- 1039 Voigt, A., S. Bony, J. L. Dufresne, and B. Stevens, 2014: The radiative impact of clouds on the
1040 shift of the Intertropical Convergence Zone. *Geophysical Research Letters*, **41** (12), 4308–4315,
1041 doi:10.1002/2014GL060354.
- 1042 Voigt, A., I. M. Held, and J. Marotzke, 2012: Hadley cell dynamics in a virtually dry snow-
1043 ball Earth atmosphere. *Journal of the Atmospheric Sciences*, **69** (1), 116–128, doi:10.1175/
1044 JAS-D-11-083.1.
- 1045 Voigt, A., and Coauthors, 2016: The tropical rain belts with an annual cycle and a continent model
1046 intercomparison project: TRACMIP. *Journal of Advances in Modeling Earth Systems*, **8** (4),
1047 1868–1891, doi:10.1002/2016MS000748.
- 1048 Wallace, J. M., Y. Zhang, and J. A. Renwick, 1995: Dynamic Contribution to Hemispheric Mean
1049 Temperature Trends. *Science*, **270** (5237), 780–783.

- 1050 Wei, H.-H., and S. Bordoni, 2018: Energetic Constraints on the ITCZ Position in Idealized Simu-
1051 lations With a Seasonal Cycle. *Journal of Advances in Modeling Earth Systems*, **10** (7), 1708–
1052 1725, doi: 10.1029/2018MS001313.
- 1053 Wiscombe, W., and S. Warren, 1980: A Model for Spectral Albedo I: Pure Snow. 2712–2733 pp.
- 1054 Wordsworth, R. D., 2016: The Climate of Early Mars. *Annual Review of Earth and Planetary*
1055 *Sciences*, **44** (1), 381–408, doi:10.1146/annurev-earth-060115-012355.
- 1056 Worsley, T. R., and D. L. Kidder, 1991: First-order coupling of paleogeography and CO₂, with
1057 global surface temperature and its latitudinal contrast. *Geology*, **19** (12), 1161–1164, doi:10.
1058 1130/0091-7613(1991)019<1161:FOCOPA>2.3.CO;2.
- 1059 Yoshimori, M., and A. J. Broccoli, 2008: Equilibrium Response of an Atmosphere-Mixed Layer
1060 Ocean Model to Different Radiative Forcing Agents: Global and Zonal Mean Response. *Journal*
1061 *of Climate*, **21** (17), 4399–4423, doi:10.1175/2008JCLI2172.1.
- 1062 Zarakas, C. M., A. L. Swann, M. M. Laguë, K. C. Armour, and J. T. Randerson, 2020: Plant
1063 Physiology Increases the Magnitude and Spread of the Transient Climate Response to CO₂ in
1064 CMIP6 Earth System Models. *Journal of Climate*, 1–44, doi:10.1175/jcli-d-20-0078.1.
- 1065 Zelinka, M. D., D. A. Randall, M. J. Webb, and S. A. Klein, 2017: Clearing clouds of uncertainty.
1066 *Nature Climate Change*, **7** (10), 674–678, doi:10.1038/nclimate3402.

1067 **LIST OF TABLES**

1068 **Table 1.** List of the idealized-continent Isca simulations used in this study, along with
1069 the land surface property values for each experiment. 49

TABLE 1. List of the idealized-continent Isca simulations used in this study, along with the land surface

property values for each experiment.

Experiment name	Description	Land albedo	Bucket depth [m H ₂ O]	Initial water in bucket [m H ₂ O]
NorthlandBright	Northern hemisphere continent with an albedo brighter than the ocean.	0.325	0.15	0.1
NorthlandDark	Northern hemisphere continent with the same albedo as the ocean.	0.25	0.15	0.1
NorthlandEmpty	Like NorthlandBright, but initialized with no water on the land surface.	0.325	0.15	0
NorthlandDry	Like NorthlandBright, but with a very small capacity for the land to hold water.	0.325	0.00001	0
Lakeworld	All-land planet with bucket hydrology modified to allow lakes to form.	0.325	0.15	0.1
NorthWestLand	Single 180°-longitude wide continent from 0-90°N, covering 25% of the planet's surface. Land surface properties same as NorthlandBright.	0.325	0.15	0.1
NorthWestLandDry	Same as NorthWestLand, but with the same land surface properties as as NorthlandDry.	0.325	0.00001	0
ThreeQuarterLand	Single 270°-longitude wide continent from 0-90°N, covering 75% of the NH (% of the total planetary surface). Land surface properties same as NorthlandBright.	0.325	0.15	0.1
ThreeQuarterLandDry	Same as ThreeQuarterLand, but with the same land surface properties as as NorthlandDry.	0.325	0.00001	0
TwoPatchLand	Two equally-spaced 90°-longitude wide continents from 0-90°N, covering a combined total 25% of the planet's surface. Land surface properties same as NorthlandBright.	0.325	0.15	0.1
TwoPatchLandDry	Same as TwoPatchLand, but with the land surface properties the same as NorthlandDry.	0.325	0.00001	0
ThreePatchLand	Three equally-spaced 90°-longitude wide continents from 0-90°N, covering a combined total 75% of the NH. Land surface properties same as NorthlandBright.	0.325	0.15	0.1
ThreePatchLandDry	Same as ThreePatchLand, but with the land surface properties the same as NorthlandDry.	0.325	0.00001	0
Aqua	Aquaplanet simulation with 20m mixed layer (no land)	–	–	–

1072 **LIST OF FIGURES**

1073 **Fig. 1.** Maps of the continental distributions used in this study. Grey areas indicate land, while
 1074 white areas indicate ocean. 52

1075 **Fig. 2.** Zonal mean temperature (a,c) and precipitation (b,d). The NorthlandBright simulation is
 1076 shown in (a) & (b) (solid lines). The anomalies for NorthlandDark - NorthlandBright
 1077 (dashed lines) and NorthlandDry - NorthlandBright (dotted lines) are shown in (c) & (d).
 1078 In a-d, black lines indicate annual mean values, while blue (red) show values for De-
 1079 cember/January/February (June/July/August) in (a,c) and cyan (magenta) show values for
 1080 February/March/April (August/September/October) in (b,d). Shading in a-d indicates ± 1
 1081 standard deviation. Panels (e,f) show the annual mean change in zonal mean relative hu-
 1082 midity (shading) and temperature (contours) for (e) NorthlandDark-NorthlandBright and (f)
 1083 NorthlandDry-NorthlandBright. Temperature contours (red/blue lines in e-f) are spaced at
 1084 1K, with red values > 0 and blue values < 0 . Only humidity values in (e,f) which differ
 1085 significantly ($p < 0.05$ using a student's t-test) are shown. 53

1086 **Fig. 3.** Zonal mean seasonal cycle of (a) precipitation, (b) evaporation, and (c) precipitation-
 1087 evaporation (P-E) for the spun-up NorthlandBright simulation; the equator/continental
 1088 boundary is marked by the solid black line. Zonal mean terrestrial water storage over the
 1089 first 6 simulation years for (d) NorthlandBright and (e) NorthlandEmpty. Zonal mean ter-
 1090 restrial water storage for (f) the full 80 year simulation of Lakeworld (note the non-linear
 1091 color bar). Cyan contour in (f) at 150mm shows the bucket capacity (i.e. fully saturated soil
 1092 moisture). 54

1093 **Fig. 4.** Seasonal cycle of zonal mean precipitation from 40°S to 40°N in (a) NorthlandBright, (b)
 1094 NorthlandDark, (c) NorthlandDry, and (d) Aqua. 55

1095 **Fig. 5.** Change in the zonal mean surface energy budget for NorthlandDry - NorthlandBright over
 1096 the course of the year. The change in downwards LW is shown in (a) while the change in net
 1097 SFC SW is shown in (b). LW emitted by the surface is shown in (c), while (d) and (e) show
 1098 sensible and latent heat, respectively. (f) shows the change in net surface energy uptake
 1099 ($E_{in} = SW^{\downarrow} - SW^{\uparrow} + LW^{\downarrow}$), where positive values indicate more energy into the surface; in
 1100 the annual mean this would be balanced by $E_{out} = LW^{\uparrow} + LH + SH$ 56

1101 **Fig. 6.** Change in the zonal mean TOA energy budget for NorthlandDry - NorthlandBright over the
 1102 course of the year. The change in net TOA SW is shown in (a) while the change in outgoing
 1103 longwave radiation is shown in (b). The net TOA energy budget (a-b) is shown in (c). The
 1104 change in the atmospheric energy source $F_{net} = TOA_{net} - SFC_{net}$ is shown in (d), where
 1105 positive indicates more energy into the atmosphere. 57

1106 **Fig. 7.** Annual mean change in surface temperature (left), latent heat flux (center), and percent
 1107 change in zonal mean specific humidity (right) for suppressing terrestrial evaporation in
 1108 various continental configurations. Thick black lines show the continental boundary. 58

1109 **Fig. 8.** The area-weighted annual mean change in (a) surface temperature and (b) latent heat flux
 1110 globally (gray), over land only (green), and over the ocean only (blue), for each continental
 1111 configuration. Small vertical black lines on each bar indicate 1 standard deviation. The
 1112 magnitude of the temperature/latent heat flux change is noted above or below each bar. The
 1113 total global land fraction for each simulation is noted along the bottom of each panel. 59

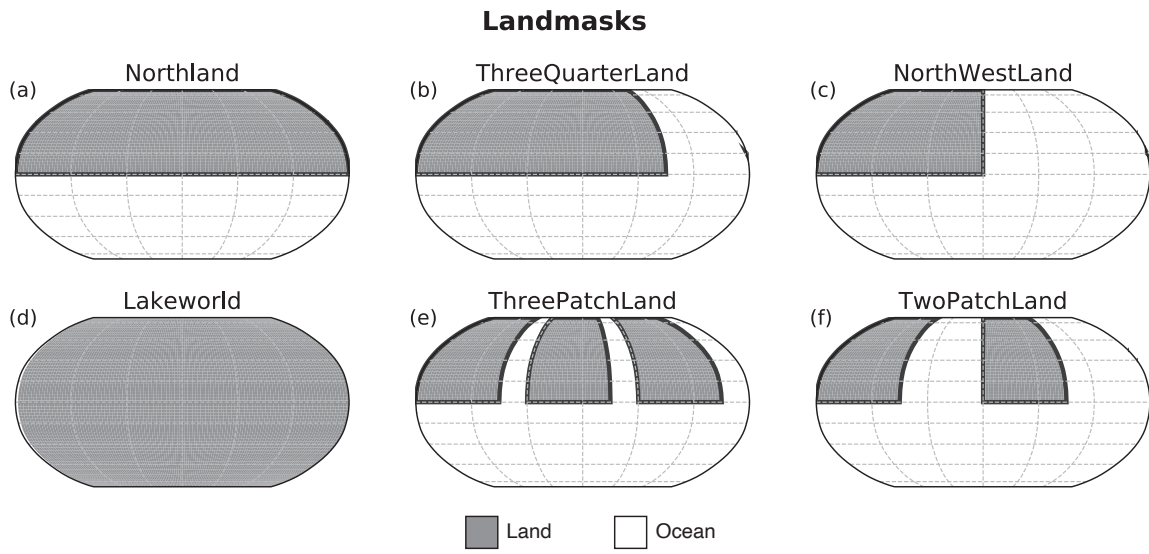
1114 **Fig. 9.** Change in surface temperature (left), change in latent heat flux (center), and percent change
1115 in zonal mean specific humidity (right) between NorthlandDark and Aqua. The annual mean
1116 change is shown in a-c, while the zonal-mean seasonal cycle is shown in d-e. 60

1117 **Fig. 10.** Top: zonal mean percent change in annual mean specific humidity for (a) NorthlandBright -
1118 Aqua and (b) NorthlandDark - Aqua. Middle: seasonal cycle of the zonal mean change in net
1119 SW absorbed at the surface for (c) NorthlandBright - Aqua and (d) NorthlandDark - Aqua.
1120 Bottom: ITCZ latitude calculated as the center of mass of zonal mean precipitation from
1121 30°S to 30°N for NorthlandBright, NorthlandDark, and Aqua, where each dot represents a
1122 single month of the year. 61

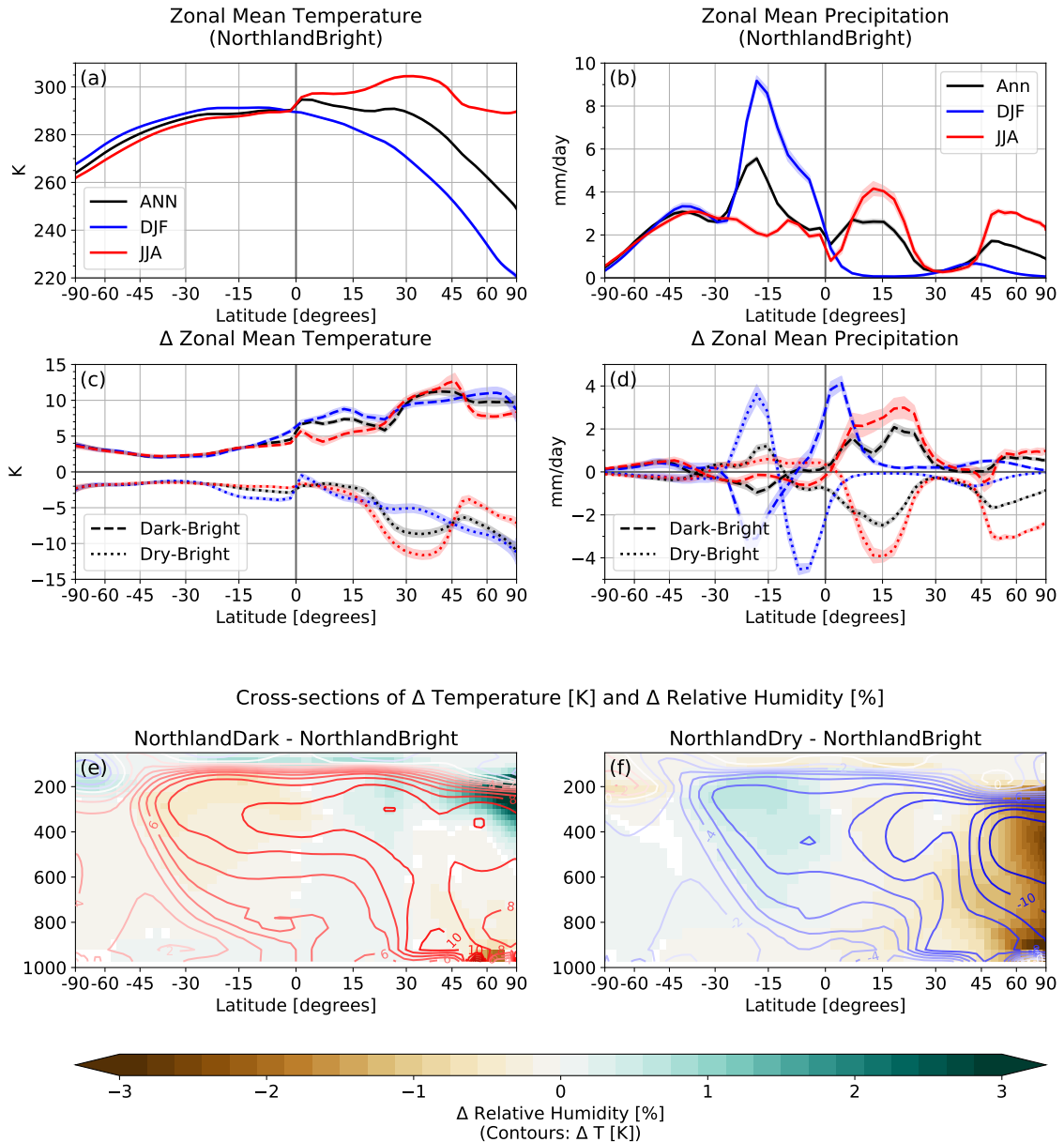
1123 **Fig. 11.** Relationship between the latitude of the ITCZ and the magnitude of cross-equatorial energy
1124 flux. The latitude of the ITCZ is calculated as the center of mass of precipitation between
1125 30°S and 30°N; the magnitude of cross-equatorial energy flux is calculated as the magnitude
1126 of meridional atmospheric energy transport at the equator. Black markers indicate annual
1127 mean values, while blue, purple, green, and red markers indicate DJF, MAM, JJA, and SON
1128 averages, respectively. Circles show values for NorthlandBright, x for NorthlandDark, and
1129 triangles for Aqua. Each individual marker shows the seasonally averaged value for a single
1130 year of the time series. NorthlandDry is not included in the regression calculations here as
1131 the ITCZ effectively collapses over the continent. 62

1132 **Fig. 12.** Zonally averaged net TOA energy flux (TOA , blue dotted line), net surface energy flux
1133 (SFC , green dash-dot line), and the atmospheric column energy source ($F_{net} = TOA - SFC$;
1134 black solid line) for the annual mean (top row), DJF (middle row) and JJA (bottom row).
1135 NorthlandBright is shown in the first column, NorthlandDark in the second, NorthlandDry in
1136 the third, and Aqua in the fourth. The total column integrated cross-equatorial atmospheric
1137 energy transport (positive northwards) for each season is noted in the lower right of each
1138 panel. 63

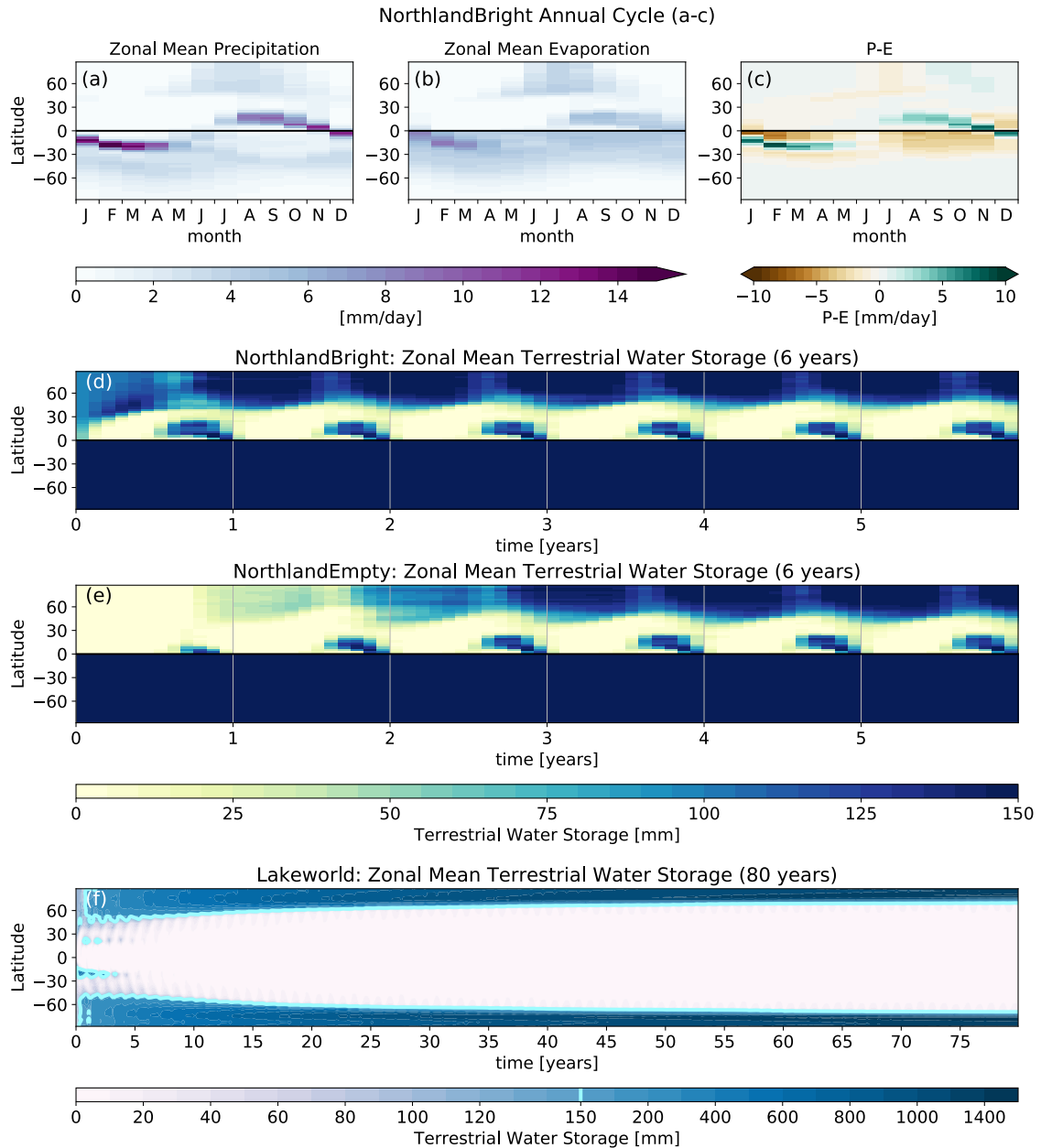
1139 **Fig. 13.** Schematic showing the surface temperature response to suppressed terrestrial evaporation
1140 for a variety of NH continental configurations. Land area generally increases from left to
1141 right, though for a given total land area, larger continents sit farther to the right on the curve
1142 than smaller, more numerous continents. Qualitative locations of suppressing terrestrial
1143 evaporation on TwoPatchLand, NorthWestLand, ThreePatchLand, ThreeQuarterLand, and
1144 Northland are shown by the maps of temperature change for each continental configuration,
1145 with the annual mean change in land surface temperature noted on each map. 64



1146 FIG. 1. Maps of the continental distributions used in this study. Grey areas indicate land, while white areas
 1147 indicate ocean.

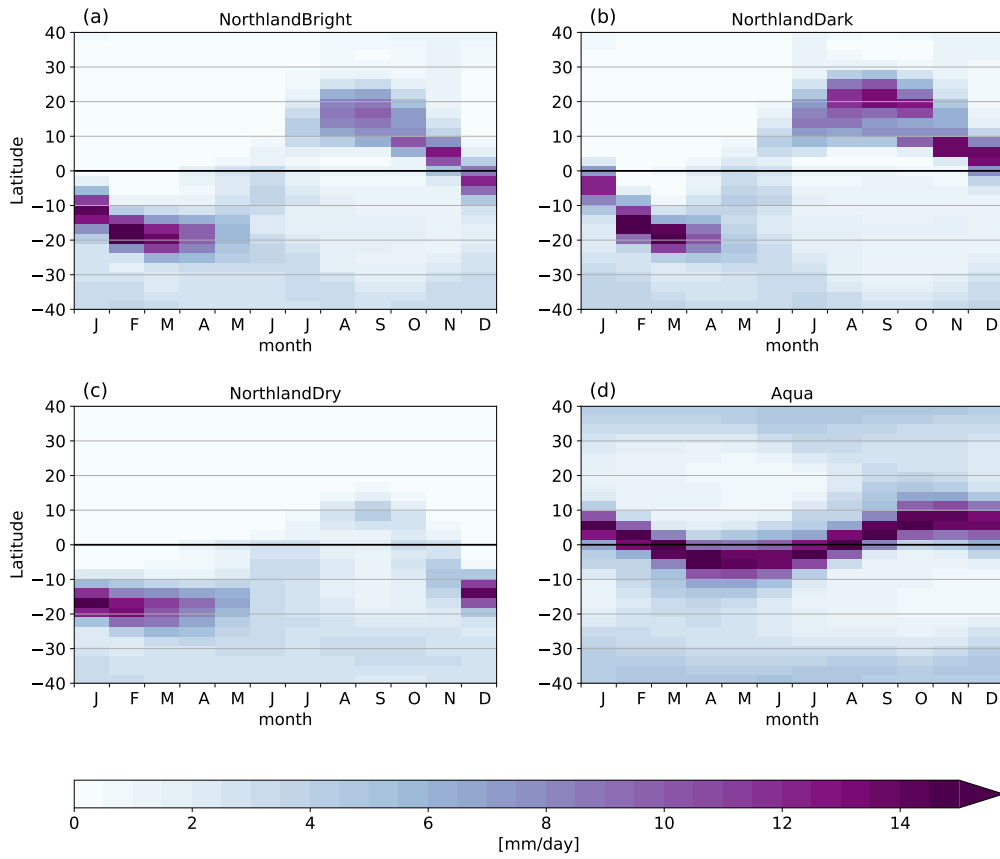


1148 FIG. 2. Zonal mean temperature (a,c) and precipitation (b,d). The NorthlandBright simulation is shown in
 1149 (a) & (b) (solid lines). The anomalies for NorthlandDark - NorthlandBright (dashed lines) and NorthlandDry -
 1150 NorthlandBright (dotted lines) are shown in (c) & (d). In a-d, black lines indicate annual mean values, while blue
 1151 (red) show values for December/January/February (June/July/August) in (a,c) and cyan (magenta) show values
 1152 for February/March/April (August/September/October) in (b,d). Shading in a-d indicates ± 1 standard deviation.
 1153 Panels (e,f) show the annual mean change in zonal mean relative humidity (shading) and temperature (contours)
 1154 for (e) NorthlandDark-NorthlandBright and (f) NorthlandDry-NorthlandBright. Temperature contours (red/blue
 1155 lines in e-f) are spaced at 1K, with red values > 0 and blue values < 0 . Only humidity values in (e,f) which
 1156 differ significantly ($p < 0.05$ using a student's t-test) are shown.



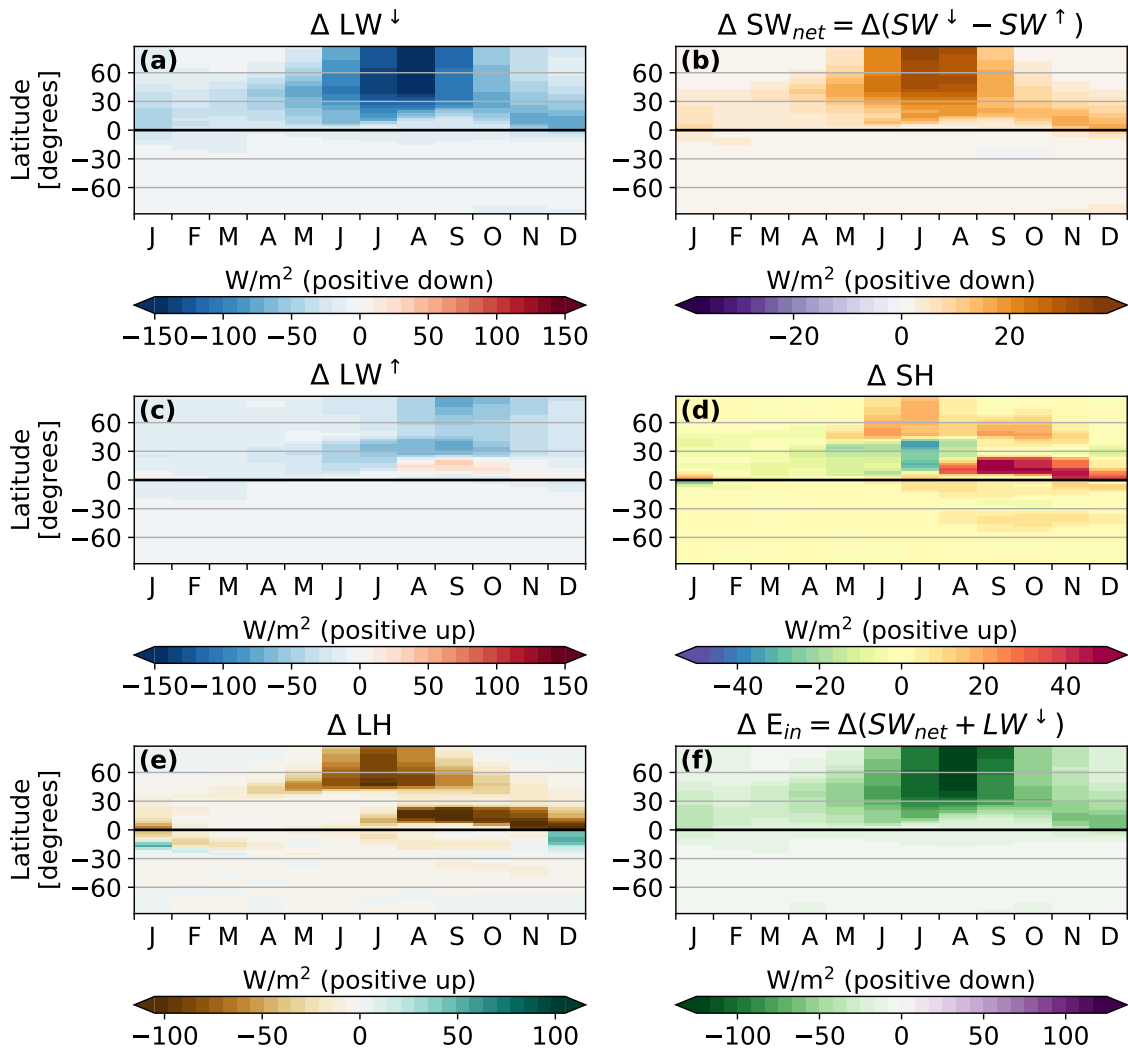
1157 FIG. 3. Zonal mean seasonal cycle of (a) precipitation, (b) evaporation, and (c) precipitation-evaporation (P-
 1158 E) for the spun-up NorthlandBright simulation; the equator/continental boundary is marked by the solid black
 1159 line. Zonal mean terrestrial water storage over the first 6 simulation years for (d) NorthlandBright and (e)
 1160 NorthlandEmpty. Zonal mean terrestrial water storage for (f) the full 80 year simulation of Lakeworld (note
 1161 the non-linear color bar). Cyan contour in (f) at 150mm shows the bucket capacity (i.e. fully saturated soil
 1162 moisture).

Seasonal Cycle of Zonal Mean Precipitation [mm/day]

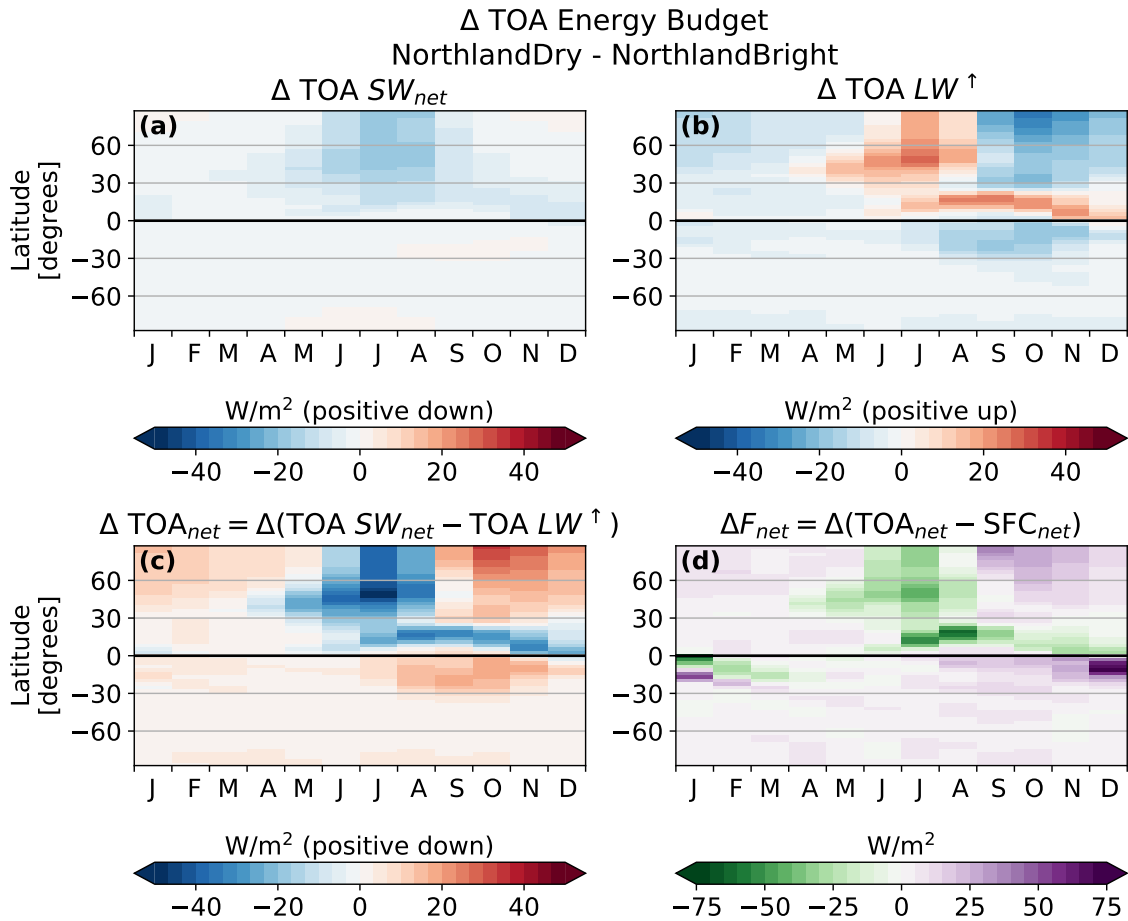


1163 FIG. 4. Seasonal cycle of zonal mean precipitation from 40°S to 40°N in (a) NorthlandBright, (b) Northland-
1164 Dark, (c) NorthlandDry, and (d) Aqua.

Δ SFC Energy Budget
NorthlandDry - NorthlandBright

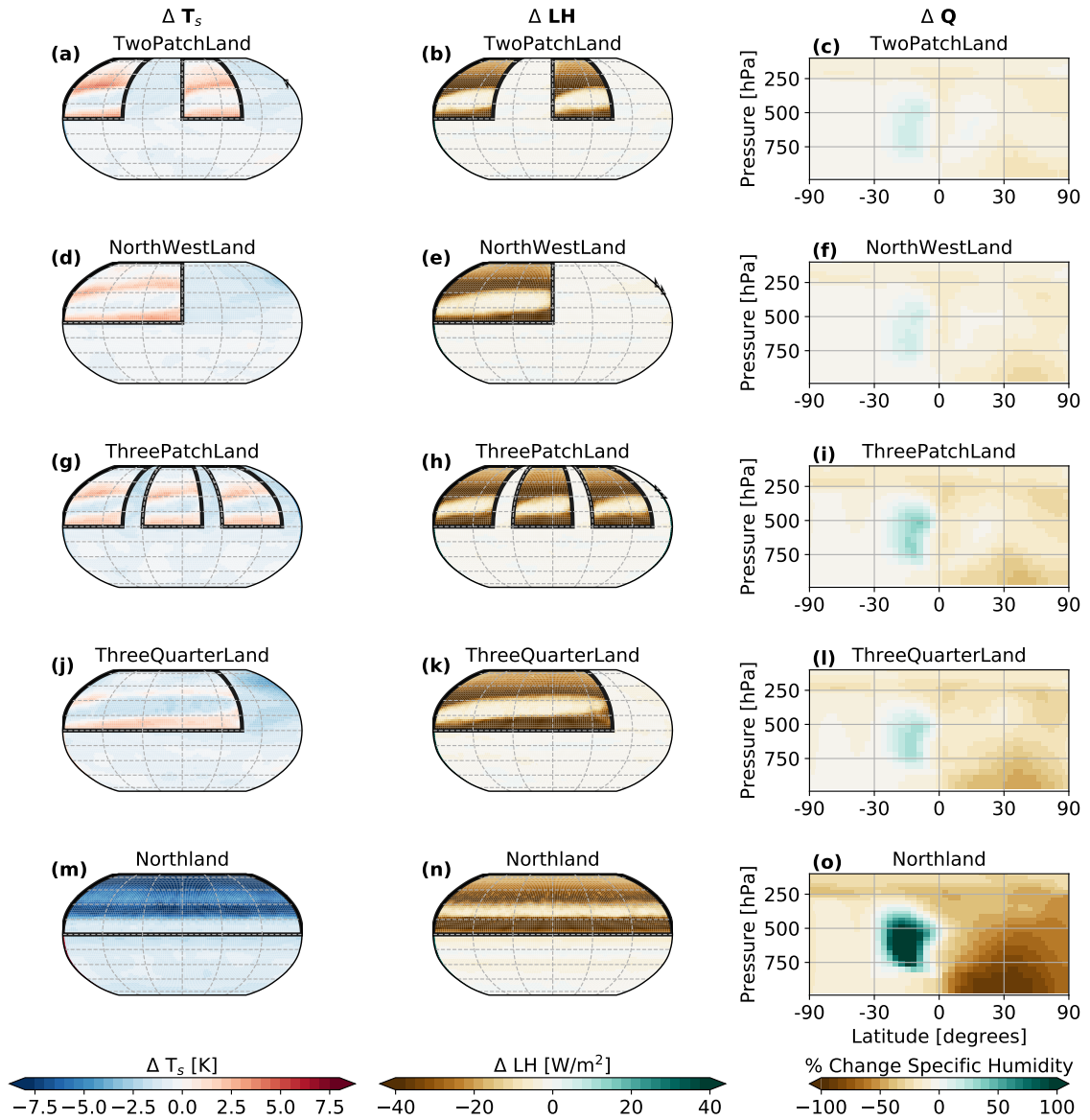


1165 FIG. 5. Change in the zonal mean surface energy budget for NorthlandDry - NorthlandBright over the course
 1166 of the year. The change in downwards LW is shown in (a) while the change in net SFC SW is shown in (b). LW
 1167 emitted by the surface is shown in (c), while (d) and (e) show sensible and latent heat, respectively. (f) shows the
 1168 change in net surface energy uptake ($E_{in} = SW^\downarrow - SW^\uparrow + LW^\downarrow$), where positive values indicate more energy into
 1169 the surface; in the annual mean this would be balanced by $E_{out} = LW^\uparrow + LH + SH$.

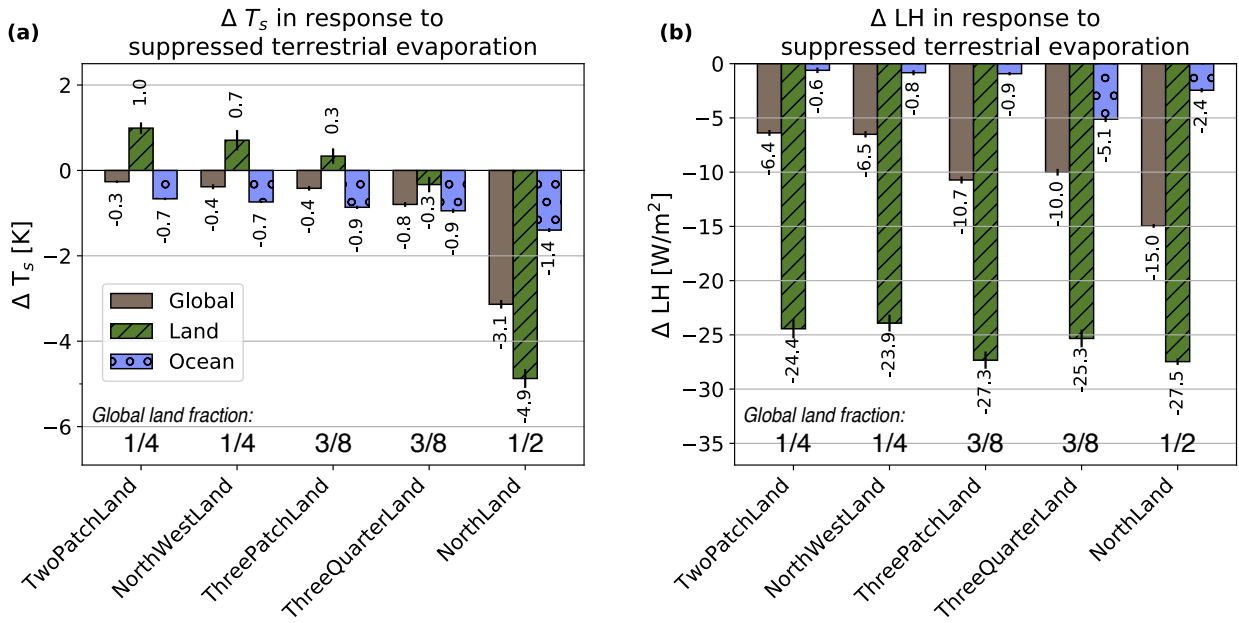


1170 FIG. 6. Change in the zonal mean TOA energy budget for NorthlandDry - NorthlandBright over the course
 1171 of the year. The change in net TOA SW is shown in (a) while the change in outgoing longwave radiation is
 1172 shown in (b). The net TOA energy budget (a-b) is shown in (c). The change in the atmospheric energy source
 1173 $F_{net} = TOA_{net} - SFC_{net}$ is shown in (d), where positive indicates more energy into the atmosphere.

**Effect of Suppressing Terrestrial Evaporation on
Surface Temperature and Specific Humidity**

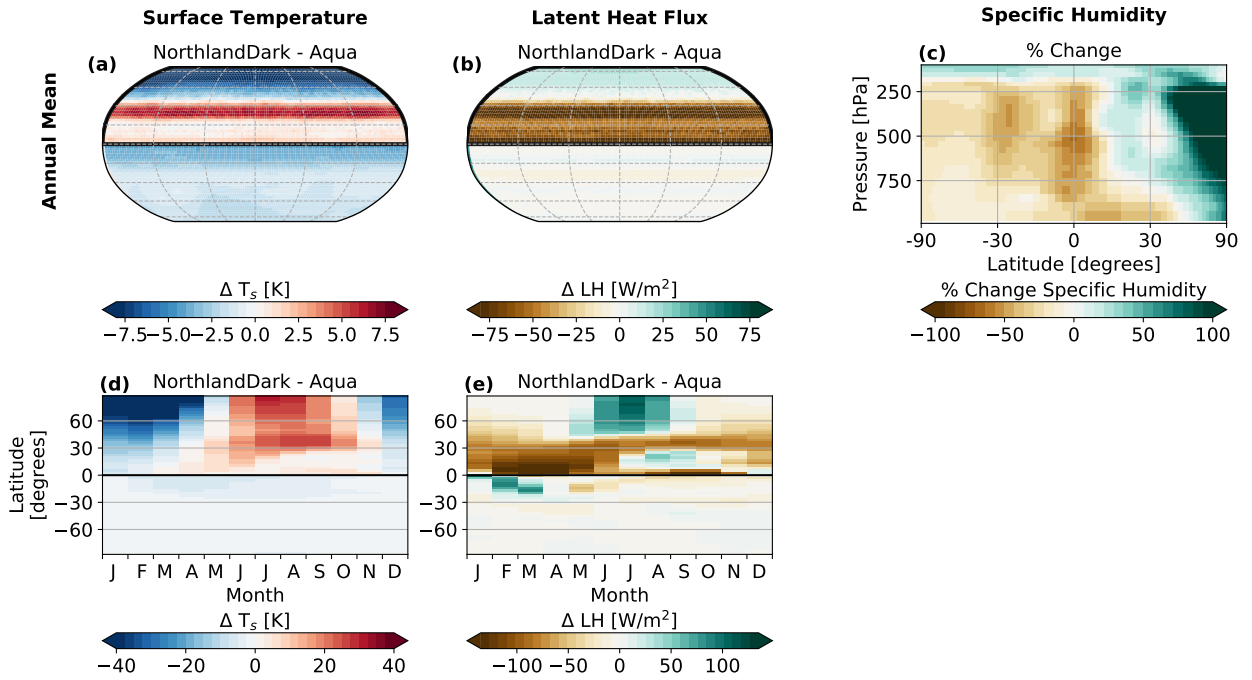


1174 FIG. 7. Annual mean change in surface temperature (left), latent heat flux (center), and percent change in
 1175 zonal mean specific humidity (right) for suppressing terrestrial evaporation in various continental configurations.
 1176 Thick black lines show the continental boundary.

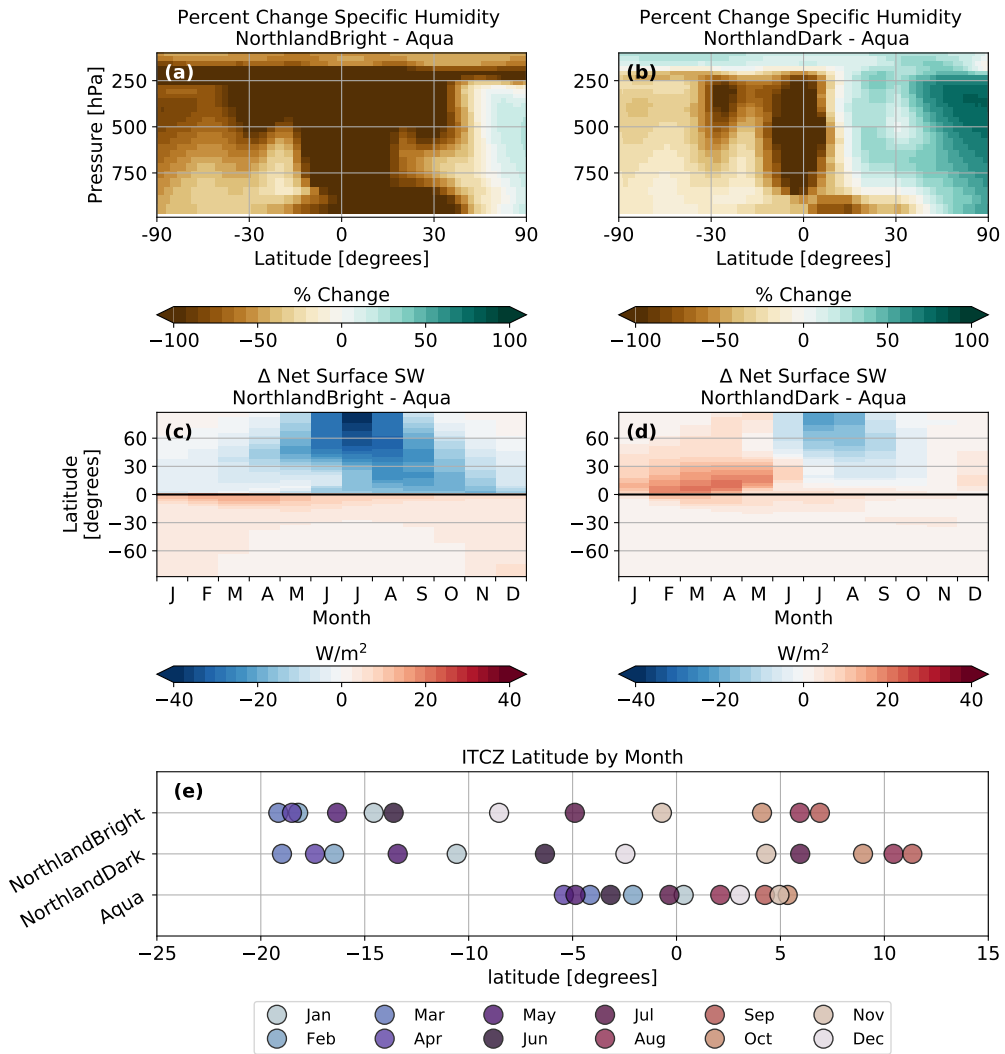


1177 FIG. 8. The area-weighted annual mean change in (a) surface temperature and (b) latent heat flux globally
 1178 (gray), over land only (green), and over the ocean only (blue), for each continental configuration. Small vertical
 1179 black lines on each bar indicate 1 standard deviation. The magnitude of the temperature/latent heat flux change
 1180 is noted above or below each bar. The total global land fraction for each simulation is noted along the bottom of
 1181 each panel.

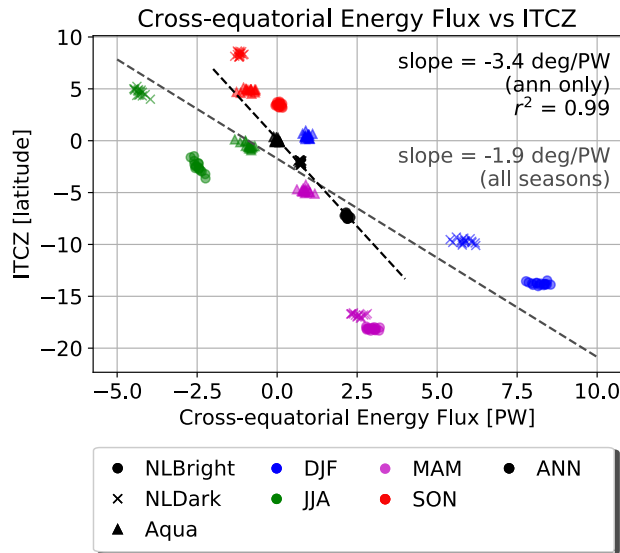
Effect of Suppressing Terrestrial Evaporation on Surface Temperature and Specific Humidity in NorthlandDark vs. Aqua



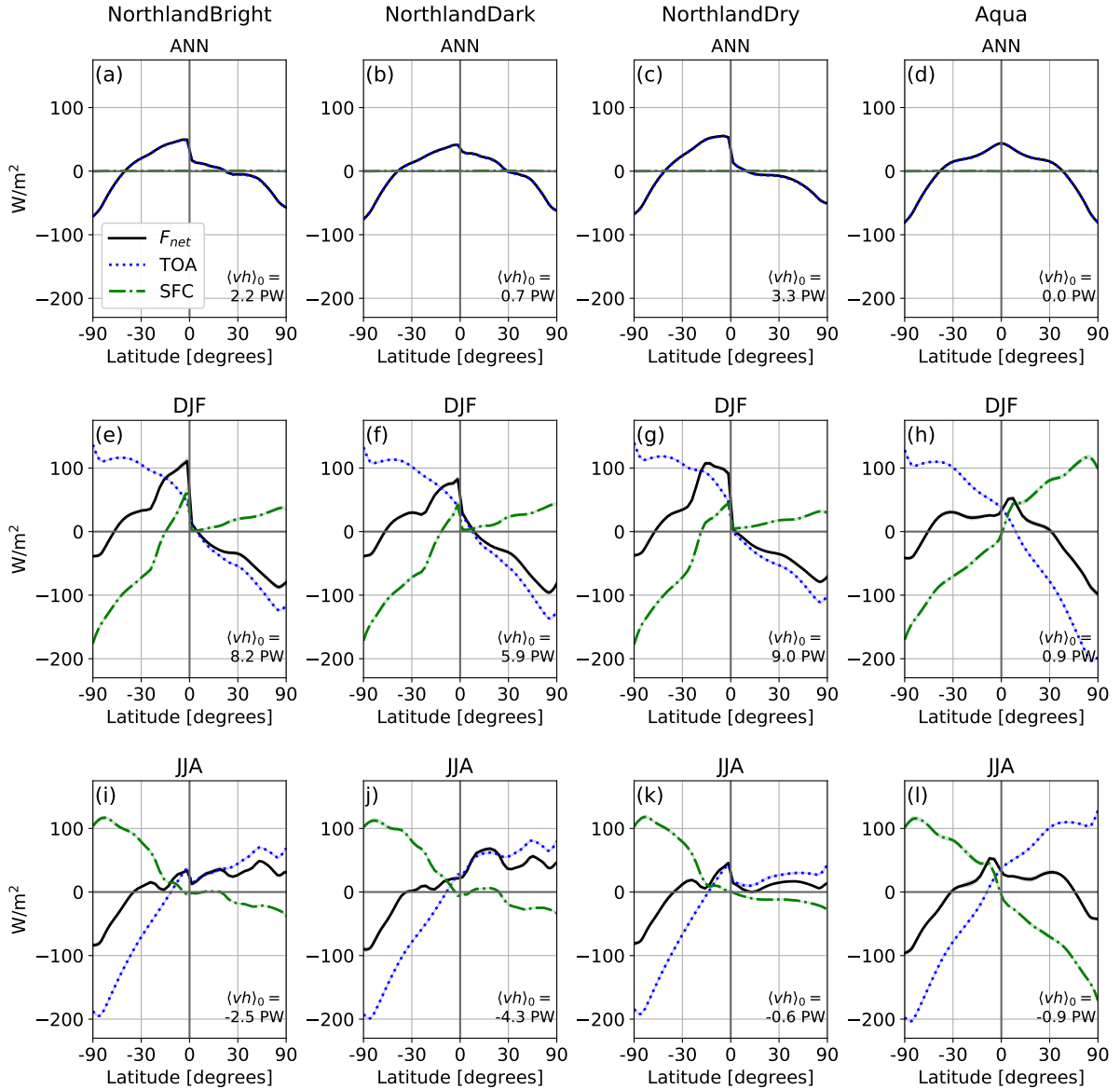
1182 FIG. 9. Change in surface temperature (left), change in latent heat flux (center), and percent change in zonal
 1183 mean specific humidity (right) between NorthlandDark and Aqua. The annual mean change is shown in a-c,
 1184 while the zonal-mean seasonal cycle is shown in d-e.



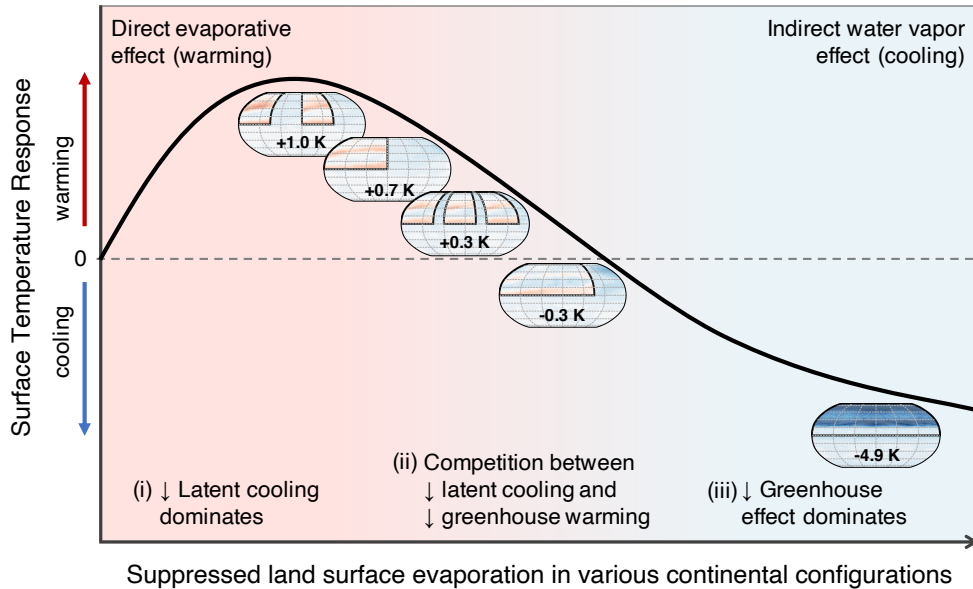
1185 FIG. 10. Top: zonal mean percent change in annual mean specific humidity for (a) NorthlandBright - Aqua
 1186 and (b) NorthlandDark - Aqua. Middle: seasonal cycle of the zonal mean change in net SW absorbed at the
 1187 surface for (c) NorthlandBright - Aqua and (d) NorthlandDark - Aqua. Bottom: ITCZ latitude calculated as the
 1188 center of mass of zonal mean precipitation from 30°S to 30°N for NorthlandBright, NorthlandDark, and Aqua,
 1189 where each dot represents a single month of the year.



1190 FIG. 11. Relationship between the latitude of the ITCZ and the magnitude of cross-equatorial energy flux. The
 1191 latitude of the ITCZ is calculated as the center of mass of precipitation between 30°S and 30°N; the magnitude
 1192 of cross-equatorial energy flux is calculated as the magnitude of meridional atmospheric energy transport at the
 1193 equator. Black markers indicate annual mean values, while blue, purple, green, and red markers indicate DJF,
 1194 MAM, JJA, and SON averages, respectively. Circles show values for NorthlandBright, x for NorthlandDark,
 1195 and triangles for Aqua. Each individual marker shows the seasonally averaged value for a single year of the time
 1196 series. NorthlandDry is not included in the regression calculations here as the ITCZ effectively collapses over
 1197 the continent.



1198 FIG. 12. Zonally averaged net TOA energy flux (TOA , blue dotted line), net surface energy flux (SFC ,
1199 green dash-dot line), and the atmospheric column energy source ($F_{net} = TOA - SFC$; black solid line) for the
1200 annual mean (top row), DJF (middle row) and JJA (bottom row). NorthlandBright is shown in the first column,
1201 NorthlandDark in the second, NorthlandDry in the third, and Aqua in the fourth. The total column integrated
1202 cross-equatorial atmospheric energy transport (positive northwards) for each season is noted in the lower right
1203 of each panel.



1204 FIG. 13. Schematic showing the surface temperature response to suppressed terrestrial evaporation for a vari-
 1205 ety of NH continental configurations. Land area generally increases from left to right, though for a given total
 1206 land area, larger continents sit farther to the right on the curve than smaller, more numerous continents. Qualita-
 1207 tive locations of suppressing terrestrial evaporation on TwoPatchLand, NorthWestLand, ThreePatchLand, Three-
 1208 QuarterLand, and Northland are shown by the maps of temperature change for each continental configuration,
 1209 with the annual mean change in land surface temperature noted on each map.